

# Micro/Nano Lasers for Biomolecular Sensing and Cellular Analysis

Xiaoqin WU<sup>1</sup>, Chunyan ZHU<sup>1</sup>, Yipei WANG<sup>1\*</sup>, and Xudong FAN<sup>2\*</sup>

<sup>1</sup>Key Laboratory of Optoelectronic Technology & Systems (Ministry of Education), College of Optoelectronic Engineering, Chongqing University, Chongqing 400044, China

<sup>2</sup>Department of Biomedical Engineering, University of Michigan, Ann Arbor 48109, USA

\*Corresponding authors: Yipei WANG and Xudong FAN E-mails: wangyp@cqu.edu.cn and xsfan@umich.edu

**Abstract:** Due to the stimulated emission amplification, lasers with excellent characteristics, including the high energy density, ultra-narrow spectral linewidth, and high directionality, are extremely favorable for sensing, detection, and imaging. Bringing these merits into the micro/nano scale, micro/nano lasers with miniaturized device sizes further enable outstanding spatial and temporal confinement, greatly boosting the light-matter interaction and bridging the size mismatch between light and biomolecules. Thanks to these advantages, micro/nano lasers have drawn widespread attention and opened new opportunities for a variety of biomedical and biochemical applications. In this paper, we review recent developments in biomolecular sensing and cellular analysis based on micro/nano lasers. We first describe the fundamental building blocks of micro/nano lasers, with discussions on gain material considerations, cavity structures, and pumping. We then review recent applications using micro/nano lasers as biosensors and bioprobes, including biomolecule (mainly proteins and DNAs) sensing, wavelength-multiplexed cell labeling/tracking/probing, and high-resolution cellular/tissue bioimaging. Finally, an outlook of the challenges and potential developments of micro/nano lasers for biological sensing and clinical applications is provided.

**Keywords:** Micro/nano lasers; cavity; biomolecular sensing; protein; DNA; cell analysis; tissue

---

Citation: Xiaoqin WU, Chunyan ZHU, Yipei WANG, and Xudong FAN, "Micro/Nano Lasers for Biomolecular Sensing and Cellular Analysis," *Photonic Sensors*, 2025, 15(1): 250123.

---

## 1. Introduction

Dating back to the 20th century, lasers, one of the greatest inventions in photonics, distinguished themselves from other light sources by their coherence, and were heralded for high directionality, irradiance, and monochromaticity. Nowadays, with the revolutionary development of lasers towards miniaturized dimensions, micro/nano lasers, combining the intrinsic merits of a coherent source

and the magic mesoscopic world, emerged as a powerful tool for a variety of applications [1–10]. When the device size reaches the wavelength scale, not only the energy consumption can be greatly reduced, but also the light interacts very differently with the matter than it does on the macroscale. For a micro/nano laser, it is possible to confine light simultaneously in frequency, time, and space, generating the lasing emission with the ultra-small mode volume, high energy density, and extremely

---

Received: 20 September 2023 / Revised: 27 December 2023

© The Author(s) 2024. This article is published with open access at Springerlink.com

DOI: 10.1007/s13320-024-0711-7

Article type: Review

narrow linewidth [5, 6, 11]. Thanks to these capabilities, micro/nano lasers have opened new perspectives for biomolecular sensing and cellular analysis, which may overcome the limitations of current fluorescence-based bioanalytical methods in terms of the sensitivity, signal-to-noise ratio, figure-of-merit, throughput, and spatial-temporal resolution [1, 3, 4, 8, 10, 12].

For conventional bioanalytical methods, characteristics of fluorescence emission (e.g., the intensity or spectrum) from fluorophores, such as dyes and fluorescent proteins, are widely used as sensing signals. However, fluorescence, originating from spontaneous emission, radiates in all directions with a relatively weak intensity and broad spectral linewidth (e.g., 30 nm–100 nm). The lack of directionality leads to inefficient signal out-coupling; the weak intensity is susceptible to background noise; the broad linewidth adversely affects the ability to distinguish a spectral shift [13–15]. Therefore, the performance of the sensing is greatly deteriorated. Meanwhile, limited by the broad linewidth, the conventional fluorescence-based approach supports no more than a few detection channels in the visible range without spectral overlapping, adding a barrier to the high-throughput and multi-channel detection [4, 16].

With a completely different emission process from that of the fluorescence, the laser features high directionality, enabling an efficient signal out-coupling for detection [8, 17, 18]. Moreover, when the pump energy is above the lasing threshold where the gain of the active medium compensates for the cavity loss, light in micro/nano lasers can circulate almost infinite roundtrips inside the cavity. By incorporating bio-materials in the gain medium or in the vicinity of the lasing mode, each time the light circulates in the laser cavity, the sensing signals or tiny changes in biological processes can be multifold amplified by the stimulated emission, offering extremely sensitive readouts of the biological changes with a high signal-to-noise ratio that can be orders of magnitude greater than the

fluorescence-based method [1, 3, 10]. Meanwhile, the light circulation results in an ultra-narrow linewidth (<1 nm), a merit desired for a high figure-of-merit (defined as sensitivity/linewidth) sensing [19, 20] and wavelength-multiplexed cell tagging and imaging [4, 16, 21].

Compared to fluorescence-based methods, micro/nano-laser-based approaches also provide versatility in sensing and detection. For example, laser emission (LE) features the nonlinear threshold behavior. The lasing output intensity has a very large contrast ( $10^2$  fold– $10^3$  fold) below and above the threshold, which can be exploited to distinguish the subtle changes occurring in a biological process [1], such as a single base mismatched deoxyribonucleic acid (DNA) during melting [22–25], metabolic activities in a single cell [26], and cell/tissue differentiation in early-stage cancer development [14, 27].

In this paper, we review the recent progress of biomolecular sensing and cellular analysis applications based on micro/nano lasers. We first elaborate three building blocks for constructing micro/nano lasers, looking into the key parameters and general consideration for the materials and structures in terms of the biocompatibility, light-biomolecule interaction, quality factor, mode volume, and exposure limit (EL) requirement. We then review various applications in biomolecular sensing and cellular/tissue analysis using different types of micro/nano lasers, as shown in Fig. 1. For the biomolecular sensing, we focus on sensing important biomolecules, such as DNAs and proteins, with different sensing mechanisms and strategies. For the cellular/tissue analysis, we review recent advances in utilizing micro/nano lasers as biological probes for cell labeling/tracking/probing and imaging platforms for cell/tissue differentiation, cancer screening, and immunodiagnosis. Finally, we discuss the future perspectives and challenges to turn micro/nano lasers into powerful tools for biomedical research and disease diagnosis.

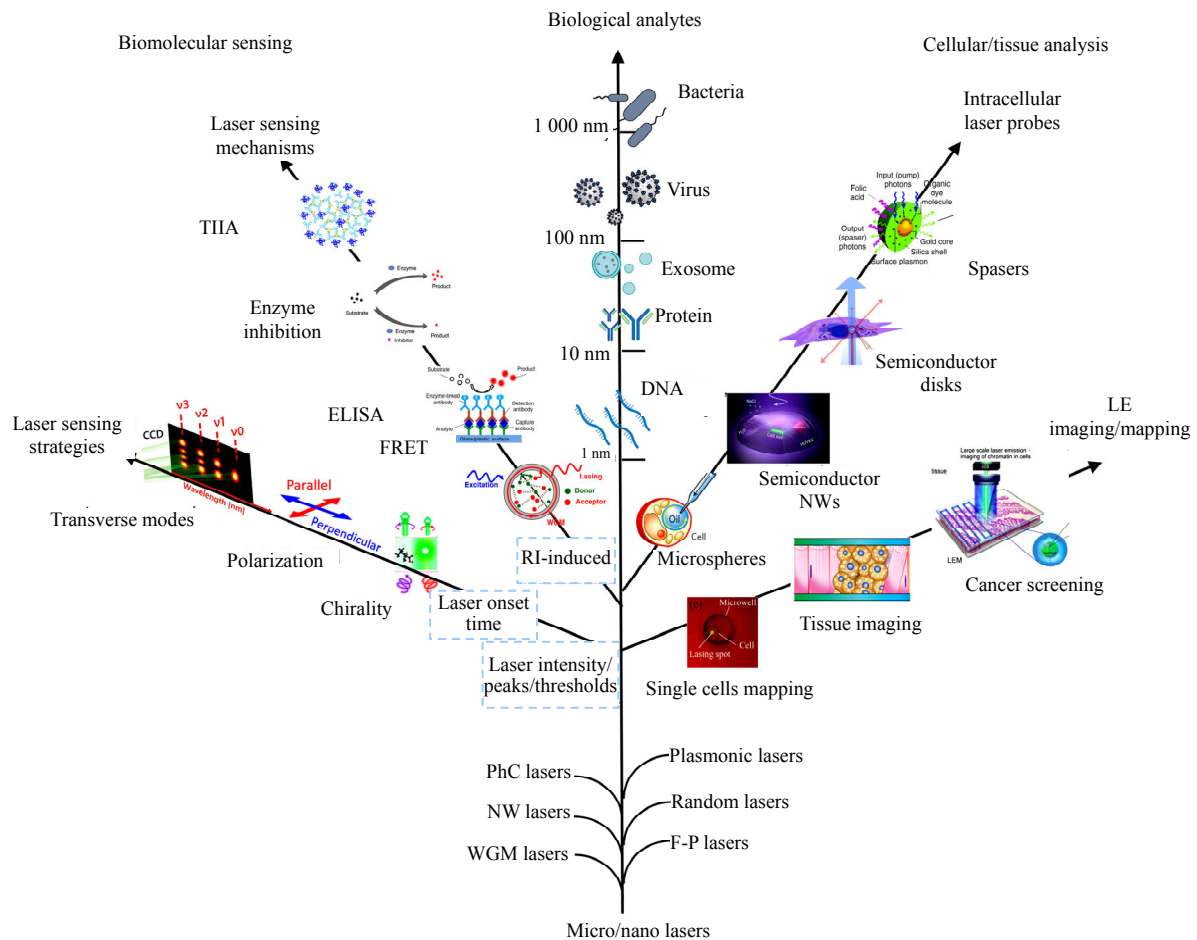


Fig. 1 Tree plot of typical micro/nano lasers and their bio-applications. The root of the tree denotes typical types of micro/nano lasers including the whispering gallery mode (WGM), Fabry-Perot (F-P), nanowire (NW), random, photonic crystal (PhC), and plasmonic laser, giving birth to various applications in biomolecular sensing of analytes ranging from DNAs to bacteria with different sensing mechanisms and strategies, as well as cellular/tissue analysis with intracellular laser probes and LE imaging/mapping. The sensing mechanisms include refractive-index (RI) induced lasing features changes, and laser intracavity sensing combined with other technologies, such as fluorescence resonance energy transfer (FRET), enzyme-linked immunosorbent assays (ELISA), enzyme inhibition, turbidimetric inhibition immunoassay (TIIA), etc. The sensing strategies include using laser intensity/peak wavelengths/thresholds, laser onset time, chirality, polarization, and transverse mode pattern as output signals. (The references of the items in Fig. 1 are listed in Appendix Table 2.)

## 2. History of biological micro/nano lasers

An early version of biological micro/nano lasers can be dated back to Gourley's work in the 1990s, in which unlabeled cells were placed inside the F-P laser cavity containing the semiconductor gain medium to passively modulate the laser characteristics [28]. Without the need for chemical staining, these biolasers became a simple and high-speed platform for cellular analysis, such as measuring intracellular biomolecular concentrations,

studying cell cycles and abnormal growth, and distinguishing individual cancerous cells from normal cells [29–31]. Since its first demonstration, the concept of the biolaser has gradually expanded from its initial definition, a laser with biomaterials (e.g., the cells mentioned above) incorporated as part of the passive cavity, to a wide range of lasers integrating biological gain media or/and embedded within biomaterials. For example, in 2010, the Fan group [32] introduced biomolecules in the gain medium (i.e., donor-acceptor dyes in a DNA scaffold) within a microcapillary-based WGM laser

cavity, in which the laser characteristics can be sensitively modulated by the DNA scaffolds, defining a novel class of actively modulated biolasers. In 2011, the Yun group [33] sandwiched single live cells expressing green fluorescent proteins (GFPs) as a viable gain medium into an F-P cavity, successfully realizing the first biological cell laser. In 2015, the Yun group [34] injected soft or hard WGM microlasers (i.e., oil, lipid droplets, or polystyrene microspheres) in cells to realize intracellular lasing and cellular probing and tagging. To date, various types of materials (e.g., fluorescent biomolecules, products of enzyme-substrate reactions, semiconductors, quantum dots, organic dyes, and rare-earth elements) [1, 3, 35, 36] and micro/nano cavities [e.g., F-P, WGM, PhCs, nanowires, and plasmonic cavities] [5, 6, 8–10, 37] have been utilized to realize biolasers, which have been successfully applied to detect a variety of bioactivities at the molecular, cellular, and tissue levels, offering a powerful tool for biomedical research with promising potential for clinical applications [1, 3, 38–40]. To promote the research in micro/nano biolasers and their applications, two Gordon research conferences entitled “Lasers in Micro, Nano, and Bio Systems” were held in 2018 (chaired by Xudong FAN & Seok-Hyun YUN) and 2023 (chaired by Malte C. GATHER), respectively, with focuses on progress in cavity designs, emerging material platforms and biomedical applications (<https://www.grc.org/lasers-in-micro-nano-and-bio-systems-conference>).

### 3. Building blocks in micro/nano lasers for biosensing

Micro/nano lasers share many similarities with conventional lasers in working principles. They consist of three major components: the pump, cavity, and gain medium. Generally, the pump provides the energy for population inversion in the gain medium, allowing light to be amplified in the form of stimulated emission; the cavity provides optical

feedback and selects the light with a certain frequency and emission direction for amplification while suppressing other light that does not meet the resonance conditions.

#### 3.1 Gain medium

As the stimulated emission occurs in the medium, the gain medium determines most of the LE characteristics. For biosensing and cellular analysis, apart from the key properties of conventional lasers (e.g., the emission wavelength, gain bandwidth, and quantum yield), the compatibility of the gain medium with the biological system, namely biocompatibility, is another important factor needed to be considered. Gain media typically used in micro/nano laser based biosensors include: fluorescent dyes or biomaterials [41–44], products of enzyme-substrate reactions [13, 45, 46], inorganic semiconductors [16, 20, 47], semiconducting (conjugated) polymers [18, 48], quantum dots [49, 50], and rare-earth elements [51, 52], which can be synthesized within or attached to biomolecules or cells. Among them, organic dyes (e.g., cyanine and rhodamine) are one of the favorable fluorescent materials with wide applications in optofluidic or solid-state micro/nano lasers, providing a promising sensing platform with excellent biocompatibility [53]. Besides, fluorescent biomaterials, including the GFP [43], monomeric Cherry (mCherry) [41], indocyanine green (ICG) [44], luciferins [42], and vitamins [54], are intrinsically biocompatible, since they can be found in living organisms [35, 55]. Moreover, they can be seamlessly merged with droplet cavities to form the biological laser operated in the liquid environment [1, 3, 35, 37], showing great potential for in-vivo sensing. These advantages aside, most fluorescent materials are subject to photobleaching that may affect their lasing and sensing performance in terms of the signal intensity, long-term stability, and repeatability. Compared to fluorescent materials, rare-earth elements (e.g., samarium, neodymium, erbium, thulium, and

holmium) [56] and organic/inorganic semiconductor materials (e.g., CdSe, HgTe, and CdSe/ZnS) [5] are usually more photostable and have been successfully demonstrated for constructing micro/nano lasers, while challenges still exist regarding how to use them in biosensing. Micro/nano lasers with rare-earth elements usually require high pump power for lasing [8], which may potentially perturb underlying biological processes. As to the semiconductors, their toxic materials in the composition restrict the application in biosensing [20, 57, 58], which might be overcome by coating a dielectric layer for protection [16]. Other semiconductor materials such as perovskite can also be used as the gain medium for bioimaging [59], while their current applications are mainly in gas sensing, since they usually suffer from the low photostability and aqueous compatibility/stability [8].

### 3.2 Cavity

Similar to conventional lasers, the gain medium for the micro/nano laser is placed inside or integrated with a cavity. Besides providing the feedback mechanism for amplification, the cavity also offers the confinement of light. Intuitively, when light is stored longer and concentrated in a smaller volume within a cavity, the light-matter interaction, an important factor for improving the sensing and detection performance, can be enhanced. The storage time corresponds to the temporal confinement of light quantified by the quality factor ( $Q$ ), and the concentration refers to the spatial confinement characterized by the mode volume ( $V$ ) [60]. A high  $Q/V$  ratio represents the ability to realize a tight and long-lasting confinement of light, and can be achieved by either enhancing  $Q$  as usually seen for dielectric cavities or reducing  $V$  as usually seen for metal cavities [61].

#### 3.2.1 WGM cavity

For dielectric cavities, ring resonators are one of the most widely used types in microlasers [8], which

utilize WGMs that were first discovered by Lord Rayleigh for sound waves in the whispering gallery of St. Paul's Cathedral around a concave surface. High-quality WGMs exist in various micro/nano structures including microcapillaries [44], microspheres [21], microdisks [16], liquid droplets [62], and microbubbles [63, 64] [Fig. 2(a)]. Due to the origin of the WGM formed by the total internal reflection at the circular boundaries, the confinement of the ring resonator depends on the refractive index (RI) contrast and size [8, 9, 65], which is thus usually of several times of  $\lambda^3$  ( $\lambda$ : wavelength) and faces challenges for further miniaturization [66]. For example, for a polystyrene microsphere (RI=1.6) widely used inside cells [15, 21, 34], as the diameter decreases below 6  $\mu\text{m}$ , the bending loss becomes significant, leading to a degradation in the  $Q$ -factor that hinders its ability to lase in an aqueous environment. Some attempts to mitigate this issue include using high RI materials [16, 47, 67] and integrating with PhC geometries [68]. For instance, the former uses GaInP/AlGaInP quantum wells to achieve a  $Q$ -factor of  $10^3$ – $10^4$  in a 750-nm-diameter and 180-nm-thick nanodisk [47]. The latter incorporates an array of holes at the perimeter of the microdisk to confine the WGM in a limited angular range, resulting in a  $Q$ -factor of  $\sim 10^5$  and a mode volume of  $0.52 (\lambda/n)^3$  in a 2.56- $\mu\text{m}$ -diameter and 325-nm-thick microdisk [68].

#### 3.2.2 F-P cavity

F-P cavities are another common resonating structure of good compatibility with fluidic channels, and thus have been widely used for constructing optofluidic microlasers for biological and biochemical sensing. Conventional F-P microcavities consist of two parallel reflective mirrors separated by a distance ranging from a few micrometers to a few hundreds of micrometers [26, 69]. Among F-P microcavities composed of mirrors with different morphology, the

plano-concave type [Fig. 2(b)(i)] can offer a relatively small mode volume while maintaining a high  $Q$ -factor [70–73]. For example, a mode volume of  $\sim 0.3 \mu\text{m}^3$  ( $\sim 1.7\lambda^3$ ) with a  $Q$ -factor of 18 000 has been demonstrated by using a plane mirror and a concave (4- $\mu\text{m}$  radius) mirror separated by 1  $\mu\text{m}$  [74]. However, such a micrometer-level concave mirror with a low surface roughness often requires a complex and high-cost fabrication process. In contrast, the plano-plano type [Fig. 2(b)(ii)] can be readily fabricated and is commonly used in the optofluidic microlasers based on F-P cavities [3, 75]. However, it lacks confinement in the lateral direction such that the mode volume is usually large. This issue can be solved by the integration with a vertical dielectric interface [Fig. 2(b)(iii)] [76] or a microsphere [Fig. 2(b)(iv)] [77], which introduces a focusing effect with an enhanced  $Q$ -factor up to  $1 \times 10^4$ – $5 \times 10^4$  and a low effective mode volume down to  $0.3 \mu\text{m}^3$ – $5.1 \mu\text{m}^3$  in an F-P cavity filled with liquids.

### 3.2.3 NW cavity

As a typical one-dimensional nanostructure, NWs serve as promising building blocks for constructing next-generation waveguiding nanophotonic devices [2, 78–80]. For an NW with a finite length, an F-P cavity is formed in the longitudinal direction due to the reflection of light between the two end facets with high reflectivity [Fig. 2(c)(i)], depending on the end facet morphology [81, 82]. Although  $Q$ -factors of NW-based F-P cavities are usually on the order of  $10^2$  [78], NWs, in contrast to conventional F-P cavities, can offer much tighter confinement in the transverse cross-section with a considerably larger field enhancement at the NW surface, greatly boosting the light-matter interaction on the sub-wavelength scale [79, 83–85]. This transverse confinement ability can be further strengthened by introducing symmetry breaking structures [86–88],

engineering cross-sectional shapes [89, 90], integration with 2D materials [91], or using coupled NW cavities [92]. An extreme optical field confinement down to the sub-nm level has recently been demonstrated in a slit cavity formed by a coupled CdSe NW pair [Fig. 2c(ii)] [92], opening new opportunities for nano lasers. For improving the longitudinal mode confinement capability, NWs can be fabricated or assembled into the photonic crystals [Fig. 2(c)(iii)] [58], Sagnac loop mirrors [Fig. 2c(iv)] [93], and ring resonators [94] with enhanced  $Q$ -factors. Apart from the aforementioned merits, when light is guided along NWs, it leaves a large amount of energy outside NWs as evanescent waves [95–97] that can be exploited for sensing either biomolecules attached onto the sidewalls or changes in the surrounding environment [57, 58]. NW-laser biosensors working in aqueous media and intracellular environments have already been demonstrated [19, 20, 59], showing high sensitivity and good biocompatibility.

### 3.2.4 PhC cavity

As an optical analogue to a crystal, where the periodic potential and band structure are introduced by the crystal atoms, a PhC cavity consists of periodic patterns of high and low RIs with a pitch on the wavelength scale [98–101]. This type of cavity can concomitantly have extremely high  $Q$ -factors and small mode volumes, allowing light to be tightly confined temporally and spatially in line [102], point [103], nanoslit defects [98], or point-shift areas [104] of the two-dimensional (2D) PhC slabs with periodic airholes [Fig. 2(d)]. For example, formed by a line defect in a 2D PhC, a nanocavity with a  $Q$ -factor of  $\sim 1.1 \times 10^7$  and a mode volume of  $1.4\lambda^3$  has been demonstrated [105]. While a PhC offers unprecedented spatial and temporal confinement, its overall size including the large periodic areas is usually on the order of 10  $\mu\text{m}$ , resulting in a total device volume larger than  $\lambda^3$  [66]. In biosensing, lasers based on

nanoslit-integrated PhC can be used to achieve ultrasensitive protein detection with an extremely low limit of detection (LOD) of  $\sim 16$  zM [106], where their confinement capability can be maximally exploited.

### 3.2.5 Plasmonic cavity

By coupling light with collective electron oscillations, plasmonic cavities, usually made of noble metals such as Au and Ag, provide the unprecedented ability to confine light on the deep-subwavelength scale, bridging the spatial mismatch between the light and biomolecules with the feature size on the nanometal level [5, 91, 107]. Although such confinement ability comes at the expense of a high loss that limits the  $Q$ -factor to the range of  $10^0$  to  $10^2$  [61], an extremely high  $Q/V$  can still be obtained due to the small mode volume beyond the diffraction limit [108]. For example, by placing an Au nanoparticle on an Au film with a sub-nm molecular spacer, a nanoparticle-on-mirror (NPoM) can be formed with a  $Q/V$  of  $3.5 \times 10^7$ , which is over an order of magnitude higher than a typical dielectric cavity such as the PhC and micropillar ( $\sim 10^5$ ), enabling the interaction between light and a single molecule into the strong coupling regime [109]. A variety of plasmonic cavities or hybrid plasmonic structures have been successfully demonstrated for plasmonic nano lasers or spasers [Fig. 2(e)], including metal nanoparticles [110, 111], nanodisks with metal layers [112, 113], semiconductor nanopatches/NWs on metal films [114–117], and metal NWs [118]. In contrast to the ones made of dielectric cavities with feature sizes limited by the diffraction limit, lasers with plasmonic cavities can be fabricated with footprints on the deep-subwavelength scale [5]. For example, the spaser made of a single Au nanoparticle with a silica shell doped with dyes is only a few tens nm in diameter [110, 111], making it an ideal candidate as a biological probe for in-vitro and in-vivo applications [111].

### 3.2.6 Other cavities

In addition to the aforementioned structures, cavities with liquid crystals (LCs) have recently attracted widespread attention [119–123]. LCs are complex fluids with good reconfigurability and biocompatibility, allowing for assembling topological structures for light manipulations in biological systems [124]. By integrating such soft topological materials with optical cavities [e.g., WGM and F-P cavities, see Fig. 2(f)], the emission of laser vector beams with diverse intensity/polarization/phase profiles can be generated and tailored, representing a novel class of coherent vector sources that can potentially be used in the study of the light-molecule interaction such as detecting nano-structural dynamics of intracavity biomolecules [119, 120].

Another approach for generating vector beams is to utilize bound states in the continuum (BIC) topological nature, and LE based on BICs is naturally a vector beam [125, 126]. Moreover, unlike conventional cavities that confine light with discrete spectral states outside a continuous spectrum of radiation, structures with BICs localize light within peculiar states lying inside the nanocylinders, showing scalability in array sizes from 20-by-20 to 8-by-8 [Fig. 2(g), left panel] [127]. In 2020, using a designed metasurface with BICs, a switchable vortex microlaser was demonstrated, enabling an ultrafast all-optical switching (1 ps–1.5 ps) between the vortex beam lasing and linearly polarized beam lasing [Fig. 2(g), right panel] [128]. In 2022, nano lasers utilizing BICs in PhCs under both continuous wave (CW) and pulsed optical pumping were demonstrated with a low threshold of  $80 \text{ W/cm}^2$  [129], extending the possibility of using nano lasers with CW pumping and low power requirement in biosensing applications (which will be further discussed in the next section).

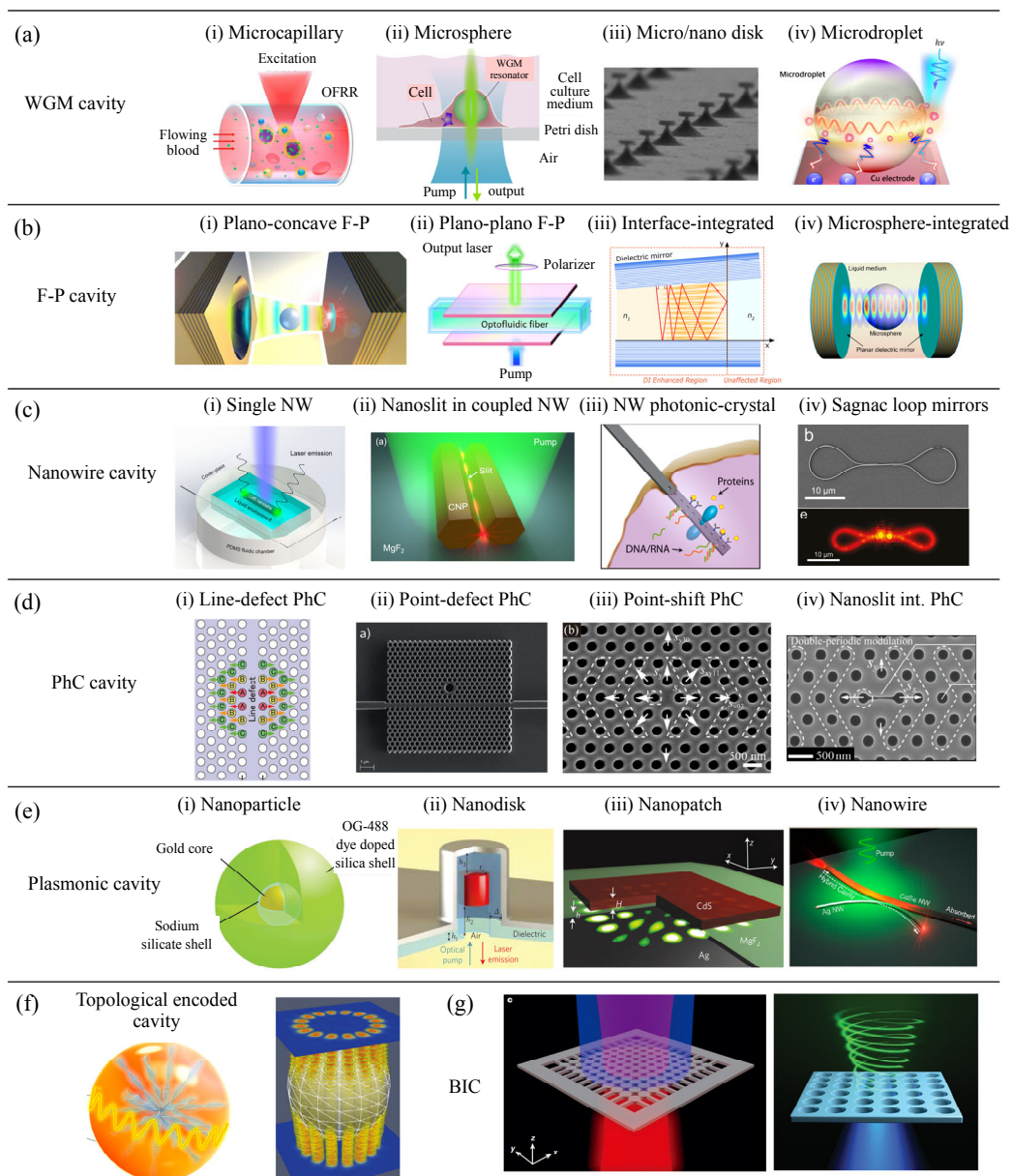


Fig. 2 Typical cavities for micro/nano lasers: (a) WGM cavities based on a microcapillary [44], microsphere [21], micro/nano disks [47], and microdroplet [62]; (b) schematics of a plano-concave [74], plano-plano [75], interface-integrated [76], and microsphere-integrated [77] F-P cavity; (c) nanowire cavities based on a single NW [19], nanoslit in coupled NWs [92], NW PhC [58], and Sagnac loop mirrors [93]; (d) ultra-confined 2D PhC cavities incorporating a line-defect [130], point-defect [103], point-shift [104], and nanoslit [131] in a regular PhC slab with periodic airholes; (e) plasmonic nanocavities based on a nanoparticle [110], nanodisk [112], nanopatch [115], and NWs [118]; (f) topological encoded cavities based on liquid crystal contained WGM [120] and F-P [121] implementations; (g) BIC cavities based on semiconductor cylindrical nanoresonator arrays [127] and perovskite metasurfaces [128].

### 3.3 Pump

Micro/nano lasers can be pumped electrically or optically. Compared to the electrical one, the optical pumping enables remote and contactless excitation, serving as the most effective method currently

available for biolasers [1]. Usually, biolasers are pumped with a pulsed laser, and a low pumping threshold is always favorable, not only for the efficient energy consumption, but also for reducing perturbations in biological media. Strategies for reducing the lasing threshold have been discussed in



many recent review articles [5, 108, 132]. Generally, for biosensing applications, to minimize damage to biomaterials, the lasing threshold should be smaller than that of the laser EL that varies from  $\mu\text{J}/\text{mm}^2$  to  $\text{nJ}/\text{mm}^2$  in the visible and near IR range, according to the factors, such as types of tissues/cells, wavelengths, and pulse durations [133]. For example, the skin has an EL of  $\sim 200 \mu\text{J}/\text{mm}^2$ , while the cornea in contrast is vulnerable to an EL of  $\sim 5 \text{nJ}/\text{mm}^2$  [133] for a visible and ns-pulsed laser. Due to their high  $Q$ -factors and/or small mode volume, state-of-art plasmonic and dielectric micro/nanolasers can realize a low threshold down to the sub- $\mu\text{J}/\text{mm}^2$  or  $\text{nJ}/\text{mm}^2$  level (e.g.,  $0.6 \mu\text{J}/\text{mm}^2$  for a hybrid plasmonic nanowire laser [118],  $0.22 \mu\text{J}/\text{mm}^2$  in a polymer ring resonator laser [134],  $25 \text{nJ}/\text{mm}^2$  in a optofluidic WGM laser [135], and  $0.93 \text{nJ}/\text{mm}^2$  in a BIC laser [129]), meeting the low EL demands for most bio-applications.

Compared to pulsed lasers for excitation, CW lasers are usually much cheaper and smaller, making them more appealing for constructing low-cost and compact instruments. Unfortunately, it is relatively difficult for micro/nano lasers to achieve lasing oscillations under CW pumping due to several possible reasons, such as the insufficient power intensity, strong heating effects, and dark/triplet state absorption for organic gain materials (e.g., dyes) [1]. One possible approach to overcome this problem is to use a metallic optofluidic cavity with a millimeter thickness, in which a room-temperature lasing under CW excitation can be realized with a threshold as low as  $2.1 \mu\text{W}/\text{cm}^2$  [136]. For miniaturized lasers on the microscale, one could resort to upconverting nanoparticles (UCNPs) with long radiative lifetimes as gain media. In 2018, utilizing a coupled structure composed of energy-loop UCNPs and a  $5\text{-}\mu\text{m}$ -diameter WGM cavity, an upconverted microlaser was demonstrated under CW pumping with a threshold of  $14 \text{kW}/\text{cm}^2$ . Such a laser can be operated in aqueous environments such as blood serum, showing great potential for biosensing and

imaging [137]. The  $\text{kW}/\text{cm}^2$  lasing threshold of the UNCP based microlasers could be further reduced to  $70 \text{W}/\text{cm}^2$  by incorporating with plasmonic cavities formed by Ag nanopillars [138].

## 4. Biomolecular sensing based on micro/nano lasers

Micro/nano lasers enable excellent spatial and temporal confinement with the greatly enhanced light-matter interaction, opening new realms for biomolecular sensing.

### 4.1 Protein sensing

As essential biological molecules in organisms, proteins play a vital role in a variety of biological activities, including metabolic reactions, the DNA replication, transporting molecules, responding to stimuli, and providing structures to cells and organisms. Selective sensing with a low LOD and accurate and high-throughput analysis of proteins are thus of great importance for medical research and disease diagnoses [139–142]. Several conventional technologies including ELISA and fluorescence immunoassay have been widely used for protein assay, while the complex operations, strong light absorption, broad emission-bands, and low contrast limit their further applications [141]. Micro/nano laser intracavity sensing emerges as a promising platform to analyze biomolecules and biological processes with superior performance.

#### 4.1.1 WGM microlaser sensing

WGM microcavities usually exhibit considerably large  $Q$ -factors that are favorable for constructing low-threshold micro/nano lasers with ultra-narrow spectral linewidths. Also, the exceptionally long photon lifetime in WGM microlasers enhances the light-matter interaction, which is thus highly suitable for biosensing. Various types of WGM microlasers based on micro-capillaries [41, 44, 143], micro-structured optical fibers [144–147], microdroplets [148–153, 152], and microspheres [154–156] have been

developed and applied to biomolecule sensing [1, 3, 8, 9]. Among them, WGM laser cavities formed by thin-walled liquid-core microcapillaries, serving as both ring resonators and microfluidic channels, have attracted a lot of attention. In 2013, an optofluidic WGM microlaser with genetically encoded fluorescent protein FRET pairs linked by length-tunable peptides as the gain medium was developed for highly-sensitive detection of protein interactions [Fig. 3(a)] [41]. Up to 25-fold reduction in the laser intensity was observed when the distance of the two proteins changed from  $\sim 30$  nm to  $\sim 6.5$  nm, while the fluorescence FRET showed only 17% reduction. Later in 2016, the first “blood laser” with clinical indocyanine green (ICG) concentrations was demonstrated in human-blood-filled microcapillaries. The dependence of the lasing behavior on three major serological components (albumins, globulins, and lipoproteins) was investigated, marking a critical step toward in-vitro diagnostics in whole blood [Fig. 3(b)] [44]. Apart from the micro-capillaries, optical fibers can also be utilized for implementing WGM laser biosensors. For instance, by adsorbing a single (or even sub-) layer of luminescent biomolecules (e.g., eGFP) on the sidewalls of a single-mode fiber, a WGM microlaser was demonstrated and its laser characteristics were found to be sensitively modulated by the biomolecular binding [43]. Later on, low-cost and reproducible optofluidic lasers were demonstrated based on micro-structured optical fibers with two [144] or one [145–147] hole in the cross-sections [Figs. 3(c)–(d)]. The latter, also called the hollow optical fiber, was used for detecting the horseradish peroxidase enzyme [145], IgG [146], and avidin [147] with LODs of 14 pM, 11 nM, and 9.5 pM, respectively. Furthermore, very recently, it was found that the WGM LE can also be achieved in the droplet-on-mirror or liquid-crystal droplet structure. In 2020, by printing hydrogel droplets on a mirror, the WGM mode lasing was achieved and applied to study FRET-related molecular interactions within the hydrogel network

[Fig. 3(e)] [149]. In 2021, a bio-responsive microlaser using dye-doped liquid-crystal droplets as a high- $Q$  WGM laser cavity was demonstrated [Fig. 3(f)], in which the lasing wavelength was modulated by surface binding molecular concentrations, interfacial energy transfer [148], and molecular electrostatic interactions [150]. In 2022, based on the similar structure and a three-dimensional (3D) deep-learning strategy, a peptide-contained droplet microlaser was demonstrated to track the amyloidogenesis process (i.e., the earlier stages of protein aggregation), which is quite challenging for the fluorescence-based imaging methods [151].

#### 4.1.2 F-P microlaser sensing

Benefitting from the simple implementation, ease of integration with various gain media, and planar configuration, F-P microcavities attract much attention in applications, such as on-chip laser biosensing [13, 45, 157], high-throughput array detection [26, 46, 70], and high-resolution laser imaging [14, 69, 158]. Among them, high-sensitivity protein sensing based on F-P microlasers has been demonstrated in the past few years. For instance, in 2014, utilizing an F-P cavity formed by two planar mirrors with a fluidic channel inserted for sample delivery, an optofluidic laser-based ELISA was demonstrated [13]. As shown in Fig. 4(a), the enzyme-substrate reaction occurs on the inner surface of the fluidic channel, generating the fluorescent product as the gain medium. Unlike conventional methods using the lasing intensity or wavelength as readout signals, this approach utilizes the laser onset time as the sensing signal that is inversely proportional to the analyte concentration inside the cavity, leading to the sensitive biomolecular Interleukin-6 detection with a large dynamic range (6 orders of magnitude) and an ultralow LOD of 1 fg/mL (38 aM). Later on, it was found that sulfide ions can slow down the enzyme-substrate reaction and delay the laser onset time. Thus, sensitive ion detection based on the

similar laser configuration was also demonstrated with an LOD of 10 nM and a dynamic range of  $\sim 3$  orders of magnitude [45]. Furthermore, based on a novel high- $Q$  wedged F-P cavity with tight lateral confinement [76], an ultrasensitive ELISA laser intracavity sensing platform with short reaction time and a small reagent volume was demonstrated to detect the protein of Interleukin-6, exhibiting an LOD of  $\sim 0.1$  pg/mL and low sample consumption of  $\sim 15$   $\mu$ L [46]. Beyond the ELISA laser biosensors, in

2019, an optofluidic laser based on TIIA was demonstrated, where the antigen-antibody complexes (ACCs) led to a scattering loss in the bulk solution [Fig. 4(b)]. By monitoring the lasing intensity responding to ACC concentration changes, the information of the analytes (antibody/antigen) could be retrieved. This TIIA was then used for IgG detection with an exceptional LOD ( $1.8 \times 10^{-10}$  g/L) and a large dynamic range of five orders of the magnitude [159].

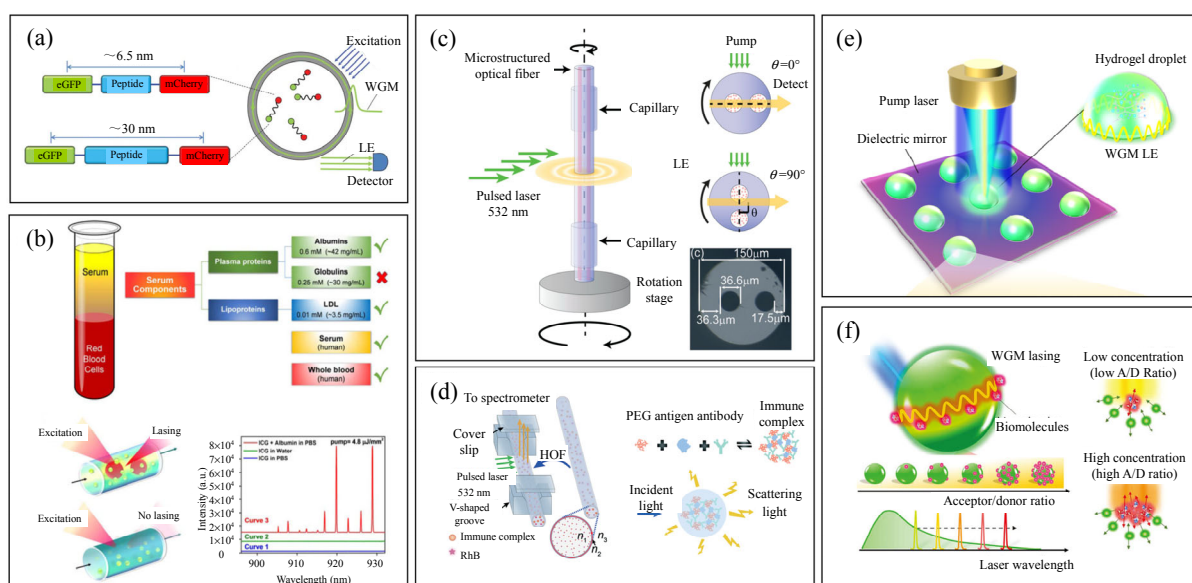


Fig. 3 WGM microlaser biosensing: (a) WGM laser biosensor based on a microcapillary for the detection of protein-protein interaction [41], (b) schematic of an indocyanine green (ICG) laser in blood [44] (upper panel: the composition of blood; bottom panel: the schematics of the blood lasers and their typical lasing spectra), (c) and (d) WGM optofluidic lasers based on micro-structured fibers with two holes (c) [144] and one hole [146] (d) in the cross-sections to fill analyte solution, (e) WGM laser based on a hydrogel droplet-on-mirror structure [149], and (f) bio-responsive microlaser with its lasing wavelength sensitive to the surface binding molecular concentrations [148].

Previous studies mainly focus on the lasing intensity, emission wavelength, lasing threshold, and laser onset time to retrieve the analyte information, while the polarization state, topology, and chirality of the laser mode can also be utilized as feedback signals. In 2020, it was found that small molecules, as well as their rotations, which could not be detected by fluorescence polarization, could be otherwise amplified and distinguished by the polarized LE [Fig. 4(c)] [75]. In 2021, by sandwiching biomimetic liquid crystal droplets with self-assembled lipid monolayers in an F-P cavity, vector laser beams were generated, and their mode topologies and polarization states reflected the

protein-lipid membrane interactions [Fig. 4(d)] [119]. Similarly, by sandwiching the self-assembled amyloids network with different structural dimensions in an F-P cavity, distinctive lasing patterns were found, offering a possible approach to exploring dynamic biological networks [160]. Besides, numerous biomolecules (e.g., amino acid, DNA, and proteins) have chirality and play important roles in biomedicine. In 2021, by encapsulating GFPs or chiral biomolecules in an F-P microcavity, a biolaser that could amplify the stimulated chiral light-biomolecule interaction was demonstrated [Fig. 4(e)], opening a new route for chiral molecule sensing and drug screening [161].

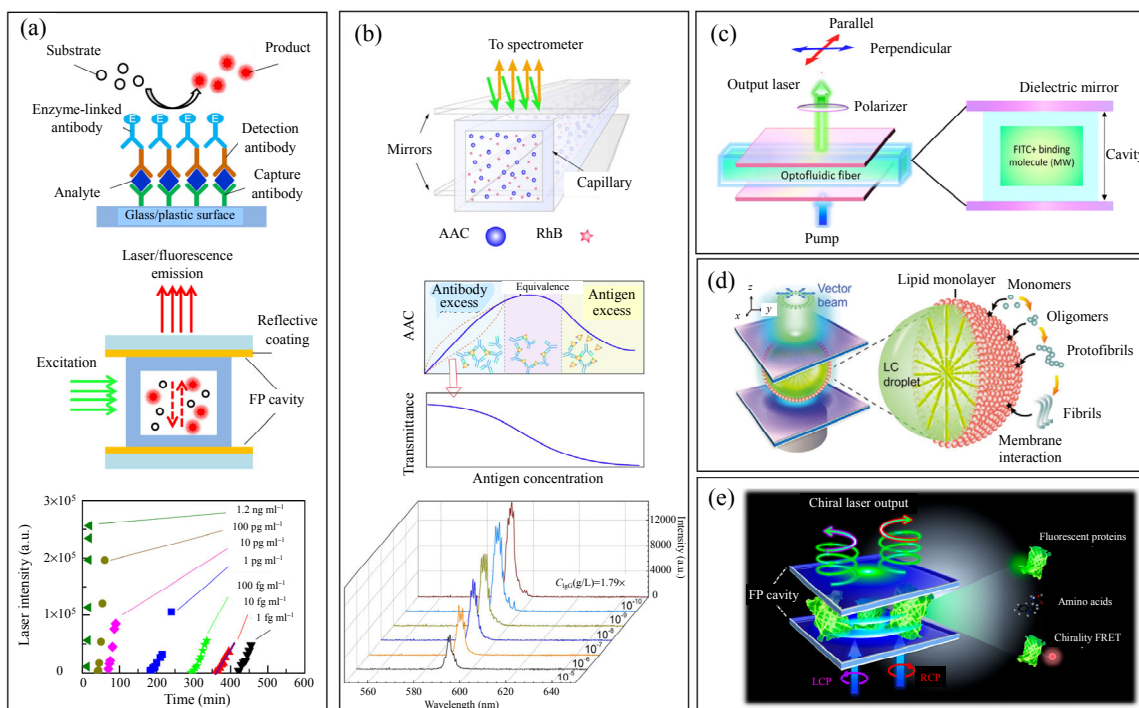


Fig. 4 F-P microlaser biosensing: (a) schematic diagram of the ELISA laser biosensor (up), typical LE from the product of the enzyme-substrate reaction (middle), and lasing intensity as a function of the catalytic reaction time for various analyte concentrations (bottom) [13]; (b) schematic of a TIIA optofluidic laser biosensor (up), TIIA-induced transmission change (middle), and laser spectra response to different IgG concentrations (bottom) [159]; (c)–(e) schematics of F-P microlaser biosensors by monitoring: (c) the laser polarization states [75], (d) laser mode topology [119], and (e) stimulated emission chirality [161].

### 4.1.3 PhC nanolaser sensing

Due to the multidimensional Bragg reflection, PhC nanocavities can confine light within a volume smaller than  $1 \mu\text{m}^3$  with a sufficiently high  $Q$ -factor  $\sim 10^4$  [98–100, 162] and thus offer an extremely strong light-matter interaction, which is particularly beneficial to high-sensitivity on-chip biomolecule sensing. One sensing principle of the PhC nanolasers is to detect the RI changes induced by the adsorbed biomolecules in the evanescent fields of the laser modes. The information of the analytes can be retrieved from the variation in the lasing wavelength. By engineering a nanoslot on a point-shift GaInAsP PhC, high-quality cavity modes with small mode volumes ( $0.2 \lambda^3$ ) can be achieved, resulting in a low threshold of  $\sim 1 \mu\text{W}$  and a single mode peak over 40 dB. The bulk RI sensitivity of the PhC nanolaser can reach 300 nm/RIU–500 nm/RIU [98]. Based on this PhC

laser configuration, the highly sensitive protein (streptavidin) assay was demonstrated with an extremely low LOD of 100 zM in the bovine serum albumin solution, corresponding to the selectivity of  $10^{13}$  [Fig. 5(a)] [106]. Recently, another sensing mechanism with superior performance was found on the GaInAsP PhC nanolaser: the surface charges on the semiconductor slab could modify the electrostatic states and thus change the lasing emission intensity and wavelength [100, 131, 104]. Such sensing mechanism can identify the negatively charged proteins (IgG) and DNA on the order of a femtomolar or lower concentration [Fig. 5(b)] [131]. Furthermore, label-free and spectral-analysis-free detection of neuropsychiatric disease biomarkers (collapsing response mediator protein 2) with an ultralow LOD of 3.8  $\mu\text{g}/\text{mL}$  was also demonstrated by using the nanoslot-incorporated PhC nanolaser [104].

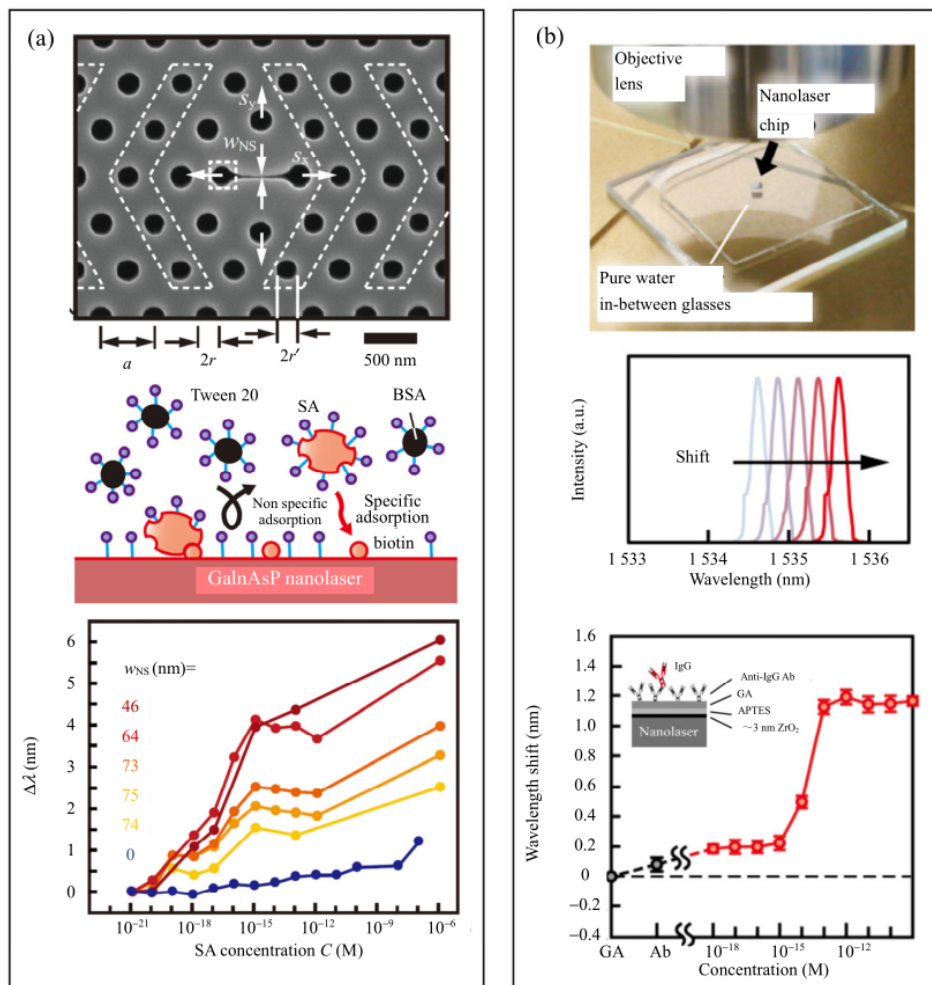


Fig. 5 PhC nanolaser biosensing: (a) structure (up), protein sensing scheme (middle), and lasing response to increasing streptavidin concentration (bottom) of the GaInAsP nanoslot PhC nanolaser biosensor [106]; (b) experimental setup for an ion-sensitive PhC nanolaser sensor (up), lasing spectra shift with the increasing biomolecules (middle), and lasing wavelength shift to different concentrations of IgG (bottom) [131].

#### 4.1.4 Distributed feedback (DFB) microlaser sensing

Owing to the planar configuration and stable single-frequency stimulated emission [163, 164], DFB microlasers can detect the binding of biomolecules to recognition layers by monitoring the lasing wavelength shift, showing great potential for on-chip label-free biosensing. A DFB laser biosensor is commonly composed by an active gain film [17, 165–169] or liquid channel waveguide [163, 170] with periodic RI changes, and a structure similar to a Bragg grating that provides an optical feedback to the laser. The bulk RI sensitivity of solid DFB lasers ranges from 20 nm/RIU–30 nm/RIU [164, 166, 171] to 70 nm/RIU–200 nm/RIU

[17, 165, 167, 172], depending on the fraction of the evanescent field outside the device that interacts with analytes. Also, it was found that evaporating a thin layer of high-index  $TiO_2$  helped enhancing the sensitivity [167, 172]. Based on an all-polymer DFB laser with two semiconducting polymers as the gain medium and a biotinylated hydrogel as the recognition layer, a label-free biosensor was demonstrated to detect the avidin-biotin interaction, showing the  $\sim 0.2$  nm lasing wavelength shift with respect to an avidin concentration of 25  $\mu\text{g/mL}$  [Fig. 6(a)] [17]. Later on, a vertically emitting organic DFB laser was used for the label-free detection of the ErbB2 cancer biomarker with an LOD of 14 ng/mL [Fig. 6(b)] [168]. In 2020,



compared with the conventional DFB biosensors using high-RI substrates, a spin-coated organic DFB laser with a low RI ( $\sim 1.34$ ) substrate exhibited a lasing threshold reduction of  $\sim 75\%$  and a 3-fold increase in the bulk sensitivity [Fig. 6(c)], achieving an LOD of 14 ng/mL for the non-specific biomolecule detection of bovine serum albumin [169]. Further improvement of the sensitivity can be realized by increasing the overlapping between the probe light and the biomolecules. A possible approach is to use a liquid-core PDMS-cladding

channel waveguide combined with a phase shifted DFB structure, in which the sensitivity as high as 560 nm/RIU–640 nm/RIU can be achieved [163, 170]. Such configuration can be extended to multi channels by using parallel liquid-core DFB lasers [173]. It also shows good compatibility with on-chip integration, which is highly desired for the point-of-care testing. For example, an all-in-one optofluidic chip integrating biomarker assay preparation and sensing was recently demonstrated for molecular biosensing assay [174].

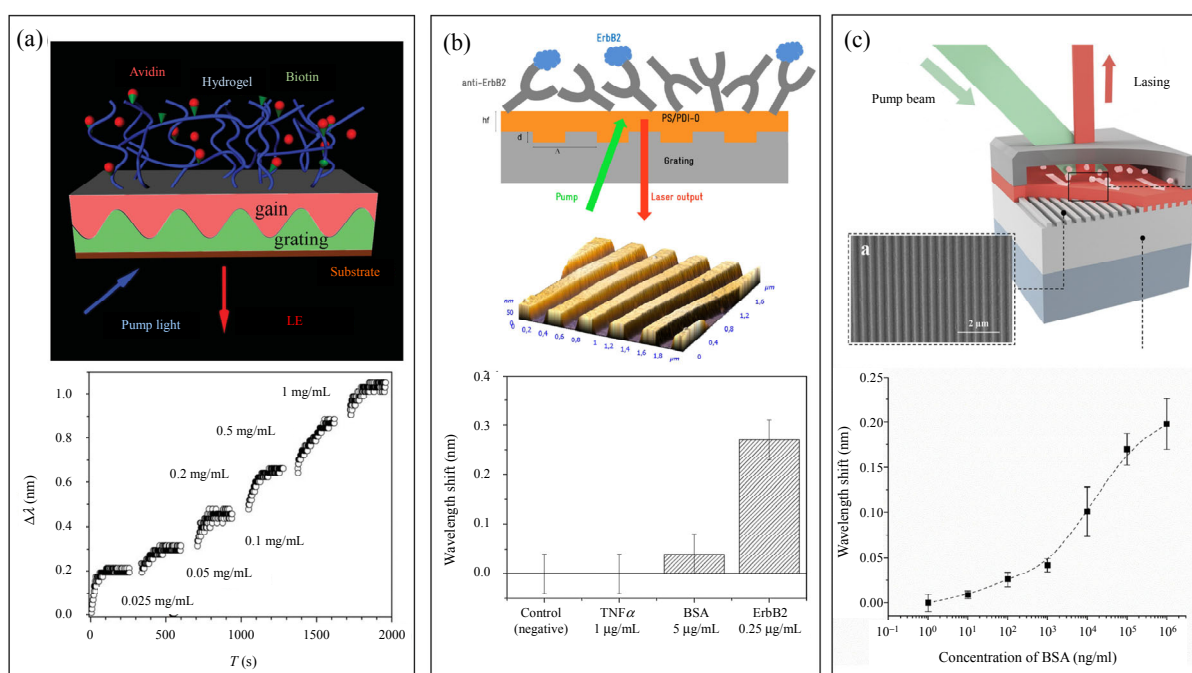


Fig. 6 DFB microlaser biosensing: (a) scheme of an all-polymer DFB laser biosensor (up) and the response of the lasing wavelength shift to the increasing avidin concentrations (bottom) [17]; (b) scheme of an organic DFB laser biosensor (up) and its lasing wavelength shift response to the ErbB2 cancer biomarker (bottom) [168]; (c) scheme of a DFB biosensor that breaks the trade-off between the sensitivity and lasing threshold by using a low-index substrate (up) and the dependence of lasing wavelength shift on different concentrations of BSA (bottom) [169].

#### 4.1.5 Random microlaser sensing

The LE can be achieved in a randomly scattering medium, where the multiple light scattering in random scatterers contributes to the optical feedback. Benefitting from the cavity-free configuration, random lasers are simple, flexible, and small in structures, and easily compatible with various biomaterials, making them excellent candidates for label-free laser biosensors. In the past few years, random lasers have been successfully demonstrated

in various biological materials, including silk [175], eggshell membranes [176], leaves [177], insect wings [178, 179], and tissues [180–184]. Variations in scatterers (size/shape/ concentration) [185–189], dye concentrations [190, 191], and RI of solvents [192, 193] can affect the random laser characteristics (e.g., lasing threshold, peak wavelength, and coherence). Such mechanisms can be utilized to design biosensors, such as *pondus hydrogenii* (pH) [194] and dopamine [195] sensors. Random lasers

for protein sensing were relatively less investigated, which might be due to the less predictable lasing peaks and thresholds. Recently in 2020, a low-cost random laser seamlessly integrated with an optical fiber was demonstrated by covering a light-emitting polymer membrane over the self-assembled randomly-distributed Ag nanoparticles on the fiber facet [196], as shown in Figs. 7(a)–7(c). The bulk RI sensitivity is  $\sim 1.24$  nm/RIU, and the specific biomolecule detection of IgG protein is demonstrated with an LOD of 0.68 nM in

Figs. 7(d)–7(e). Owing to their cavity-free structure, random lasers were also used in cell studies [197, 198] and biomedical diagnosis, such as distinguishing between healthy and cancerous tissues [184, 199, 200]. Recently, random lasing in label-free living cells was achieved by adding the biocompatible gain medium into the cell culture medium and using cells as random scatterers. The lasing spectrum was utilized to study cell apoptosis, opening new opportunities for rapid cytometry of apoptosis [197].

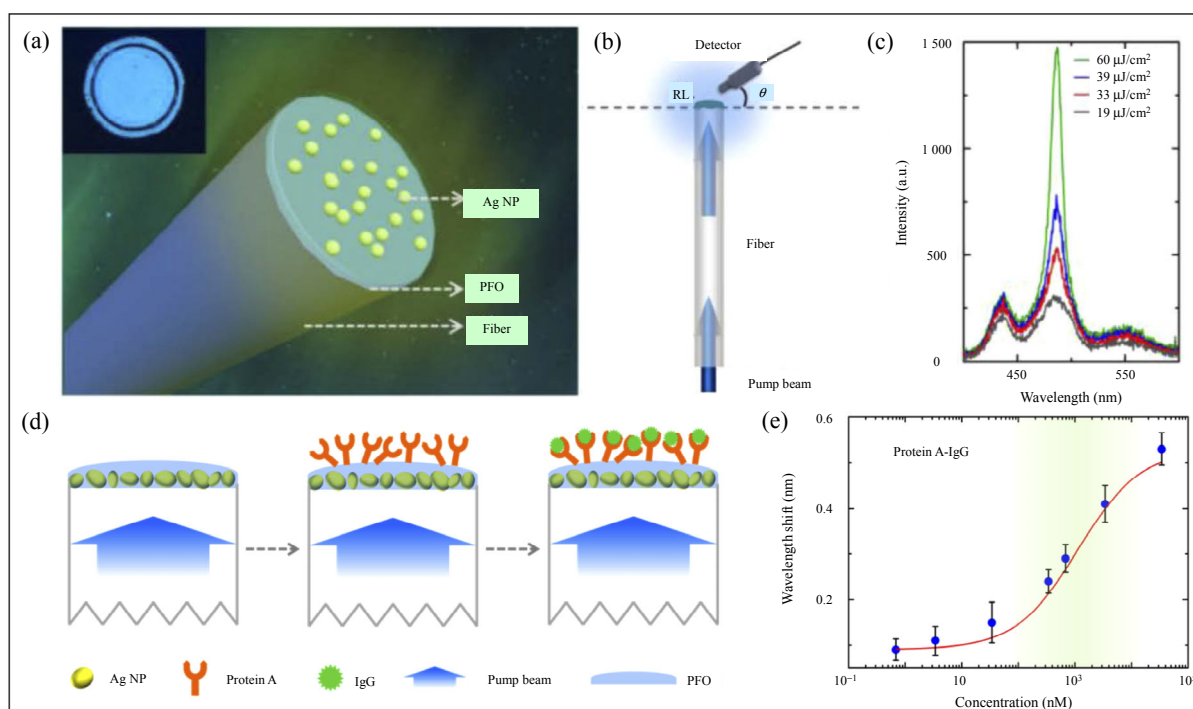


Fig. 7 Random laser biosensor on the fiber facet for detecting biomolecules [196]: (a) schematic diagram of a plasmonic random laser, (b) experimental setup, (c) lasing emission spectra under different pump power densities, (d) schematic diagram of IgG detection, and (e) lasing wavelength shift as a function of the IgG concentration.

## 4.2 DNA sensing

DNA is one of the most potent biomolecules, which has the unique function of storing an organism's genetic code and is critical for all cellular functions and heredity. A DNA sequence may have a base-pair change due to some biological processes, such as single-point mutation and cytosine methylation. Sensitive and accurate detection of these DNA sequential differences at the level of single-base mismatch gives important information

for clinical research and numerous genetics-related fields. The first DNA biolaser, consisting of DNA scaffold donor-acceptor dyes as the gain medium and a thin-walled liquid-core microcapillary as the high- $Q$  ring resonator, was demonstrated in 2010 with a low lasing threshold down to the level of  $\mu\text{J}/\text{mm}^2$  [32]. As shown in Fig. 8(a), based on this microlaser configuration, highly specific intracavity detection of DNA is performed with the capability of distinguishing two DNA sequences that only have a single base mismatch [22, 23], which is beyond the

discrimination ability of the fluorescent counterparts [201–203]. Besides, DNA-switchable optofluidic WGM microlasers controlled by the DNA Holliday junctions [204] and DNA tetrahedra [205] were reported with the capillary-based WGM resonators, suggesting microlasers as a promising platform for precisely detecting the DNA conformational changes. In these microcapillary-based WGM laser cavities, however, only 0.1%–1% of the gain molecules in the bulk solution contribute to the lasing action, and the rest gain molecules simply add to the background fluorescence that deteriorates the LE quality or the bioanalysis sensitivity [43]. To address this issue, in 2016, a novel optofluidic WGM laser system based on a single-mode optical fiber was utilized to detect a target DNA sequence in a digital manner with ultra-low sample consumption [24]. In this system, only a single layer of DNA-labeled dye molecules was attached to the fiber surface, successfully suppressing the intrinsic fluorescence background. Apart from WGM cavities, F-P microcavities were also explored for DNA laser biosensors, providing the whole-body interaction between light and

biomolecules that significantly enhanced the sensitivity and suppressed the background fluorescence [70]. In 2018, a highly sensitive DNA melting analysis approach based on F-P optofluidic lasers [Fig. 8(b)] was demonstrated, in which a single-base mismatch for long DNA sequences (~130 bases) could result in ~20% difference in the laser threshold and ~40% difference in the lasing output slope [25]. In 2020, based on an F-P microcavity formed by two mirrors and a dye-doped liquid-crystal matrix [Fig. 8(c)], a DNA self-switchable microlaser was demonstrated, where the conformational change in DNA, serving as switching power to modify the orientation of the liquid crystals, caused the variations in the lasing wavelength and intensity [206].

Except for the DNA and protein sensing, micro/nano lasers can be used to detect larger biomolecular analytes with higher sensitivity, such as exosomes [153], viruses [8, 207, 208], and bacteria [37, 209–211] (Fig. 1), owing to the stronger interactions between the laser light and the

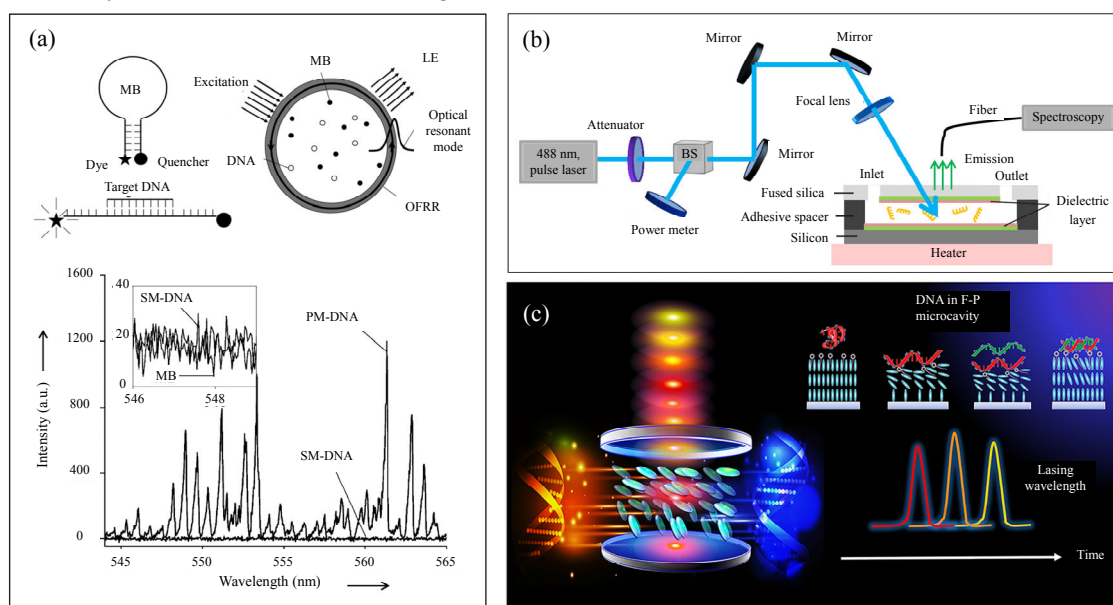


Fig. 8 DNA sensing using microlasers with WGM and F-P configuration: (a) distinguishing single-base-mismatch DNA by monitoring laser spectra (up) [23] and the fluorescence/lasing spectra of the perfectly matched (PM) DNA and single-base mismatched (SM) DNA, respectively (bottom); (b) schematic diagram and experimental setup of an F-P optofluidic laser for DNA melting analysis [25]; (c) DNA self-switchable microlaser based on a liquid-crystal matrix sandwiched in an F-P microcavity, where the DNA hybridization changes the liquid crystal orientation [206].



analyte. For example, by monitoring the changes in the self-heterodyning beat note of the split lasing modes, single Influenza A virion can be detected by a toroidal-shaped WGM microlaser [207]. Similarly, in-vivo lasing can also be achieved at the single

bacterial level with great potential for live-cell sensing [210].

In summary of this section, some representative micro/nano laser-based biosensors and their typical sensing mechanisms and features are listed in Table 1.

Table 1 Representative micro/nano laser-based biosensors and their sensing mechanisms and features.

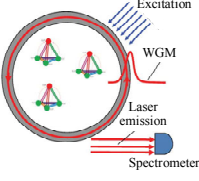
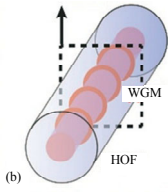
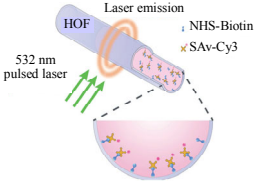
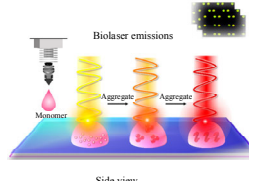
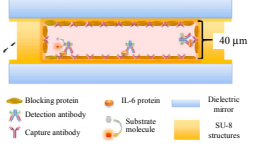
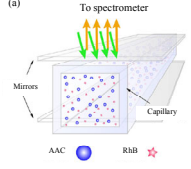
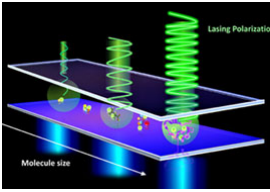
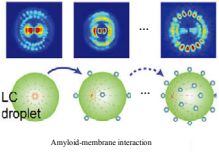
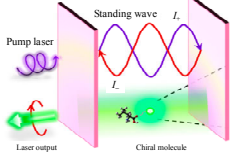
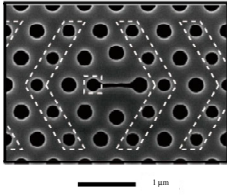
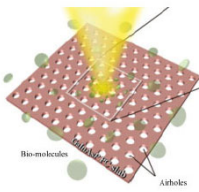
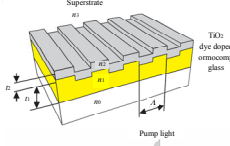
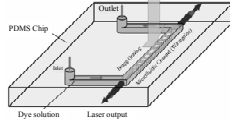

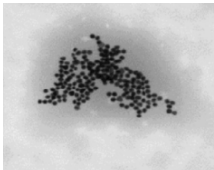

Laser cavity	Device example	Sensing/lasing mechanism	Biomolecular analytes	Performance/features
WGM: microcapillaries or single-mode fibers		Combine FRET and laser intracavity detection	Protein interactions [41, 44, 149, 150] DNA [22, 23, 32, 204, 205]	LOD=0.36 pM [150] distinguishing DNA sequential differences at the level of single-base mismatch [22, 23]
WGM: hollow-core fibers		Laser-based arrayed colorimetric detection	Enzyme	LOD=14 pM, high throughput (5 channels) [145]
WGM: thin-walled fibers		Combine immunoassay and laser intracavity detection [146, 147]	IgG, avidin	LOD=9.5 pM, ease to mass production, disposable [146]
WGM: droplets on the mirror		Combine deep-learning and laser imaging	Protein folding	High throughput, real-time monitoring [151]
F-P: two mirrors		Combine ELISA and laser intracavity sensing [13, 46]	Interleukin-6	LOD=38 aM, dynamic range=6 orders of magnitude [13]
F-P: capillary inserted between two mirrors		Combine TIA and laser intracavity sensing [146, 159]	IgG	LOD=1.8×10 <sup>-10</sup> g/L, dynamic range=5 orders of magnitude [159]
F-P: two mirrors		Laser polarization measurement	Small molecules	Study small molecules and their molecular rotation [75]

Table 1 (Continued) Representative micro/nano laser-based biosensors and their sensing mechanisms and features.

Lasers cavity	Device example	Sensing/lasing mechanism	Biomolecular analytes	Performance/features
F-P: liquid crystal droplet inside		Vector laser beam: laser topology measurement	A $\beta$ -lipid interactions	Study subtle protein-lipid membrane interactions [119]
F-P: two mirrors		Laser chirality measurement	Chiral molecules	~100 $\times$ enhanced by the LE compared with the fluorescence counterpart [161]
PhC: shifted points or nanoslots incorporated		RI-induced lasing wavelength shift [98, 106]	Streptavidin	Mode volumes $\sim 0.2\lambda^3$ , sensitivity=300 nm/RIU–500 nm/RIU, LOD=100 zM [106]
PhC: nanoslot incorporated		Surface charge induced lasing changes [100, 131, 104]	Charged proteins or DNAs	LOD is in the range of 16 zM–255 fM [100]
DFB: periodic gain films		RI-induced lasing wavelength shift [17, 165, 166, 168] TiO <sub>2</sub> layers enhancing the sensitivity [167, 172]	Avidin, cancer biomarkers	Sensitivity=95 nm/RIU LOD=7.5 $\times 10^{-6}$ RIU [167]
DFB: periodic liquid waveguides		Bragg grating lasing wavelength shift [163, 170, 173, 174]	nucleic acids	Sensitivity is in the range of 560 nm/RIU–640 nm/RIU [163]
Random lasers: silk-based		Gain parameters change the lasing intensity and FWHM	pH	Sensitivity: ~200 times that of an identical fluorescence-based sensor [194]
Random lasers: gold nanoparticles incorporated		Dopamine-induced aggregation of gold nanoparticles	dopamine	LOD=100 nM and dynamic range is 100 nM–10 mM (five orders of magnitude) [195]
Random lasers: gold nanoparticles incorporated		RI-induced lasing wavelength shift	IgG	Sensitivity=1.24 nm/RIU, LOD=0.68 nM, and dynamic range is 84 nM–12 $\mu$ M [196]

\*: Insert figures adapted from (top to bottom) [205], [145], [147], [151], [46], [159], [75], [119], [161], [100], [100], [167], [170], [194–196]).

## 5. Cellular analysis

### 5.1 Stand-alone micro/nano lasers

Owing to laser characteristics including the narrow linewidth and high brightness, micro/nano lasers in living cells enable the massively multiplexed cell tagging, ultrasensitive intracellular probing, as well as super-resolution bioimaging [59], thus spurring widespread attention. These tiny laser particles inside cells may help us to better understand the cellular heterogeneity in biology and are potential candidates for single-cell analysis. In 2015, by embedding high-quality micro WGM resonators (e.g., oil/natural lipid droplets, or polystyrene beads) inside living cells [Fig. 9(a)], the intracellular laser action was demonstrated, which was applied to chart the cytoplasmic internal stress

with the sensitivity of  $20 \text{ pN} \cdot \mu\text{m}^{-2}$  (20 Pa) and tag thousands of individual cells by lasing wavelength multiplexing [34]. The diameters of these microlasers fell in the range of  $6 \mu\text{m}$ – $12 \mu\text{m}$  and their lasing spectra served as barcode-type labels that enable identifying and tracking of individual migrating cells uniquely [21, 34]. Afterwards, the organic-SiO<sub>2</sub> core-shell nanowire microlasers [212], semiconductor [20] [Fig. 9(b)] or perovskite [59] nanowire lasers, and plasmonic nano lasers [213] were also internalized into the living cells through natural endocytosis to demonstrate cell tagging, probing or imaging with significantly reduced sizes and perturbation to the cells. Following research in 2017 showed that the laser microbeads could be fabricated with biomaterials and implanted in the

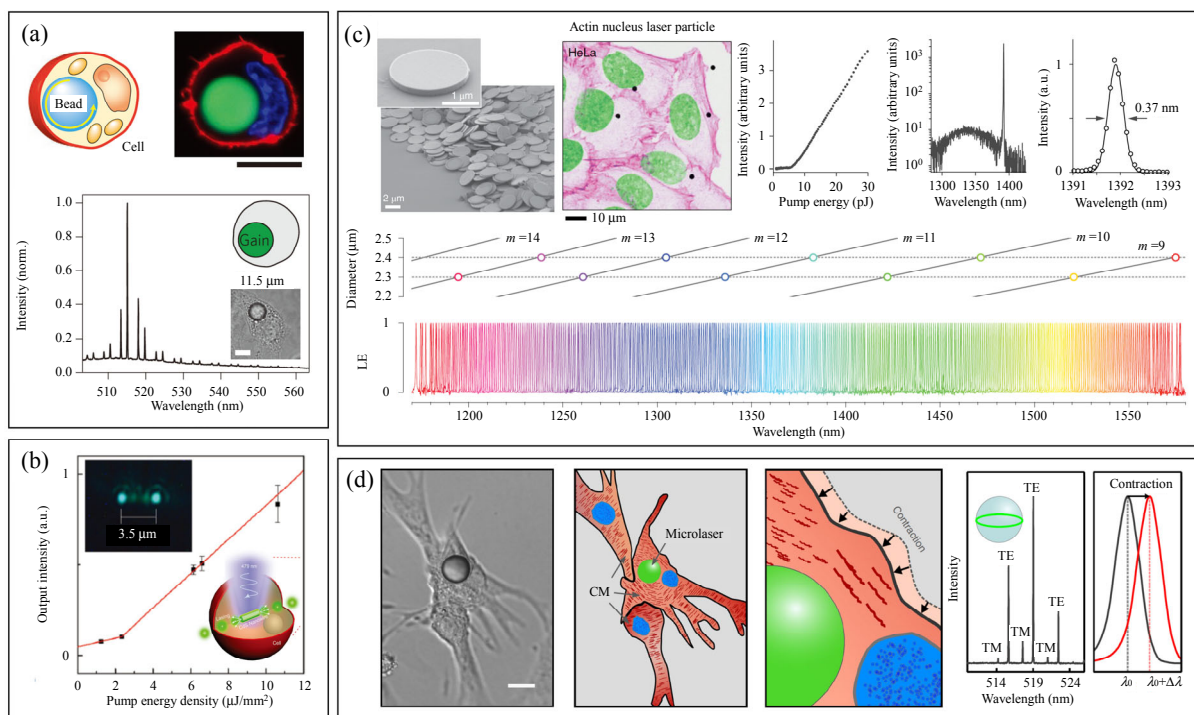


Fig. 9 Stand-alone micro/nano laser particles enabling intracellular sensing and detection: (a) embedding dye-doped polystyrene beads into cells to detect internal stress dynamics and enable cell tagging [34]: schematics (up) and the typical lasing spectrum of the intracellular microlaser (bottom); (b) semiconductor nanowire lasers internalized into cells for intracellular environmental probing [20]: lasing threshold curve of the intracellular laser; (c) intracellular semiconductor microdisk lasers with narrow single-mode lasing peaks and wide tunable range of 1170 nm–1580 nm [16]: the SEM image of the microdisks, fluorescence image of HeLa cells containing microlasers, lasing threshold curve, lasing spectrum, and Gaussian fit of the lasing peak, respectively (upper panels, from left to right); the lasing spectra of 400 microdisk lasers, exhibiting continuous wavelength tunability from 1170 nm to 1580 nm (bottom); (d) monitoring contractility in cardiac tissue using lasing polystyrene microspheres [15]: the microscopy image, schematics, a magnified view that visualizes the contractile movement of the cell around the microsphere, the lasing spectrum of a microlaser, and the lasing spectrum changes due to the cell contraction, respectively (the panels from left to right).

cornea, skin, and blood for light-based diagnostics and therapies [214]. To further minimize microlasers down to the sub- $\mu\text{m}$  level in 3D, nanodisk lasers composed of high-gain GaInP/AlGaInP quantum wells were integrated into cells with the ultralow lasing threshold and excellent spectral stability, which allowed cell-tracking through micro-pores and provided an ideal platform to study cell migration and cancer invasion [47]. In 2019, intracellular semiconductor microdisk lasers were demonstrated with narrow single-mode lasing peaks that could be continuously tuned in a wide range of 1 170 nm–1 580 nm, and the real-time tracking of thousands of individual cells was demonstrated in a 3D tumor model over several days (Fig. 9(c)) [16]. In 2020, by using biointegrated microsphere lasers as intracellular probes, the contractility of the cardiac tissue with cellular resolution was monitored with high spectral sensitivity in the live zebrafish and rat heart tissue [15].

## 5.2 Imaging and mapping on the cellular and tissue level

Apart from the stand-alone micro/nano lasers mentioned above, another way to achieve cellular lasing and analysis is to sandwich cells in an F-P cavity. The first single cell biological laser using such configuration was demonstrated in 2011 with GFPs gene-expressed by living cells [33]. Ever since, the F-P cavity based cell lasers emerged as a powerful tool to study cell cycle stages [26], ion flux [215], cell secretion [216], and cell classification [217]. In 2017, based on a microwell array containing cells sandwiched between two mirrors [Fig. 10(a)], high-throughput long-term monitoring of individual cells (e.g., cell sizes, cycle stages, and ploidy) was demonstrated [26]. In 2020, by placing neurons inside an F-P cavity and detecting the LEs [Fig. 10(b)], an optical imaging and recording system for ion influx in single neurons and neuronal networks was demonstrated with sub-cellular resolution [215]. The detection

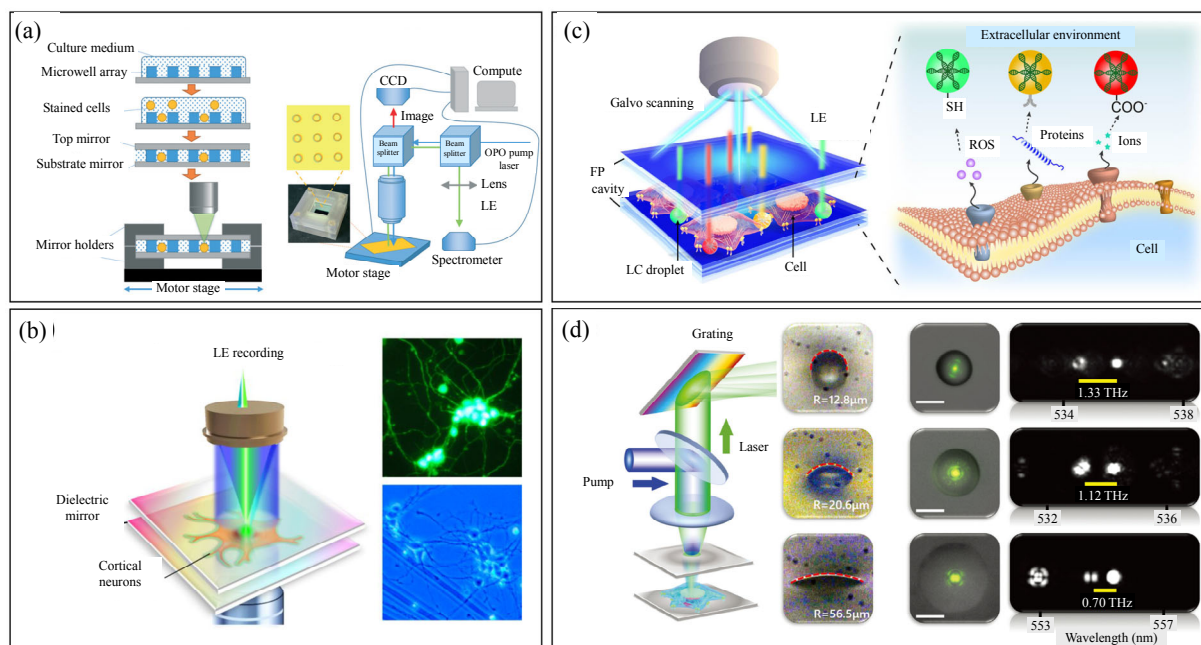


Fig. 10 Cellular lasing and analysis by sandwiching cells between F-P cavities: (a) integrated microwell array platform for the detection of cell sizes, cycle stages and ploidy [26]; (b) neuron lasers for the detection of ion flux in the neuronal networks [215]; (c) multifunctional laser imaging of cell secretion in extracellular environment by sandwiching dye-doped liquid crystal droplets and living cells in an F-P cavity [216]; (d) hyperspectral laser imaging of transverse laser modes for cell analysis: schematic, side-views of droplets (mimicking cells), LE patterns, and hyperspectral images of laser modes, respectively (left to right columns) [217].



sensitivity was proved to be improved more than 100-fold compared with fluorescence-based measurement. In 2022, by introducing hybrid liquid crystal resonators and pancreatic cancer cell lines into an F-P cavity [Fig. 10(c)], multifunctional laser imaging of cancer cell secretion (e.g., cellular metabolism, proteins, redox oxygen species, and ions) was demonstrated [216]. In 2022, utilizing the spectral information of transverse laser modes as output signals [Fig. 10(d)], the biolasers with individual cells sandwiched between F-P cavities were demonstrated for investigating cell adhesion and classification [217].

As a group of cells, a tissue usually carries out a specific function, which is of more practical value since it closely resembles the complex biological environment in a living organ or body. Since the progress has been made to achieve lasing in single cells, tissue lasers and analysis can be realized in a similar way with F-P cavities. For example, in 2017,

with fluorophore-stained tissues sandwiched in a high- $Q$  F-P cavity [Fig. 11(a)], a versatile tissue laser platform was developed, in which the laser output could reflect the tissue structure/geometry, tissue thickness, and staining concentration [69]. Meanwhile, based on the similar configuration, a scanning-laser-emission-based microscope that could map the lasing emission from nuclear biomarkers in human tissues with sub-micron spatial resolution ( $<700$  nm) and a narrow lasing band (a few nanometers) was demonstrated [Fig. 11(b)], enabling the high sensitivity for distinguishing cancer and normal tissues [14]. In 2018, by sandwiching an SU8 spacer to fix the F-P laser cavity length, a highly robust tissue laser platform was demonstrated with reproducible and stable lasing performance regardless of the tissue thickness, which was further used for distinguishing cancer and normal lung tissues by their corresponding lasing thresholds [158]. Later on in 2019, still using the

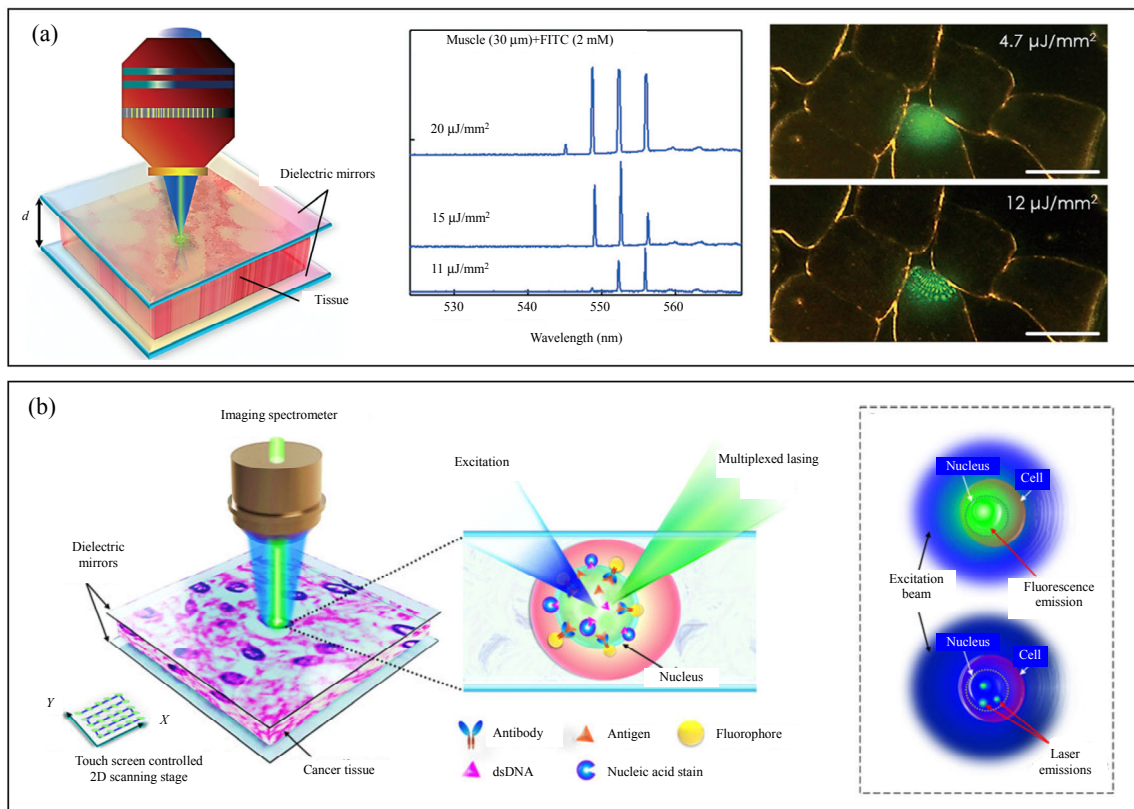


Fig. 11 Lasing and imaging with tissues sandwiched in F-P cavities: (a) schematic of a tissue laser (left), the lasing spectra under different pump fluence (middle), and the microscopy images of the muscle tissue below and above the lasing threshold (right) [69]; (b) laser-emission imaging of nuclear biomarkers in human tissues with sub-micron spatial resolution [14].

F-P microcavities with tissue analytes inserted, a rapid scanning laser-emission microscopy was constructed to detect abnormal changes in cell nuclei for early diagnosis of cancer [27]. Very recently, random lasers were also utilized for cell/tissue differentiation [180, 183, 197] and cancer diagnosis [182, 199].

### 5.3 Multimodal imaging and sensing

To date, no single imaging technique is perfect: the widely used fluorescence microscopy (FM) may suffer from broad emission bands and low contrast; the LE imaging provides high imaging contrast and spatial resolution, while limited by the imaging depth; photoacoustic (PA) imaging and optical coherence tomography (OCT) offer an excellent platform for 3D imaging in tissues but have a low multiplexing capability. In this context, multimodal imaging, a hybrid method with more than one imaging technique, offers a great opportunity for combining the advantages of these existing

techniques together to enhance the imaging capability and performance. Owing to their laser characteristics, physical sizes, and photothermal (PA)/photoacoustic properties, micro/nano lasers are considered as promising multimodal agents. In 2017, spasers made of plasmonic nanoparticles were demonstrated as multimodal cellular nanoprobe. Along with the LE signal, PT and PA signals were significantly amplified due to nanobubbles generated by the light absorption, showing an excellent multimodal capability for biomedical applications [Fig. 12(a)] [213]. In 2019, ultrasound modulated droplet lasers were demonstrated with deformable WGM cavities, providing a possible solution to break the optical diffusion barrier with the enhanced imaging depth for high-resolution and high-sensitivity deep tissue imaging [Fig. 12(b)] [218]. In 2020, a dual-modality imaging system was developed with intracellular nanowire lasers providing the enhanced OCT and FM signals

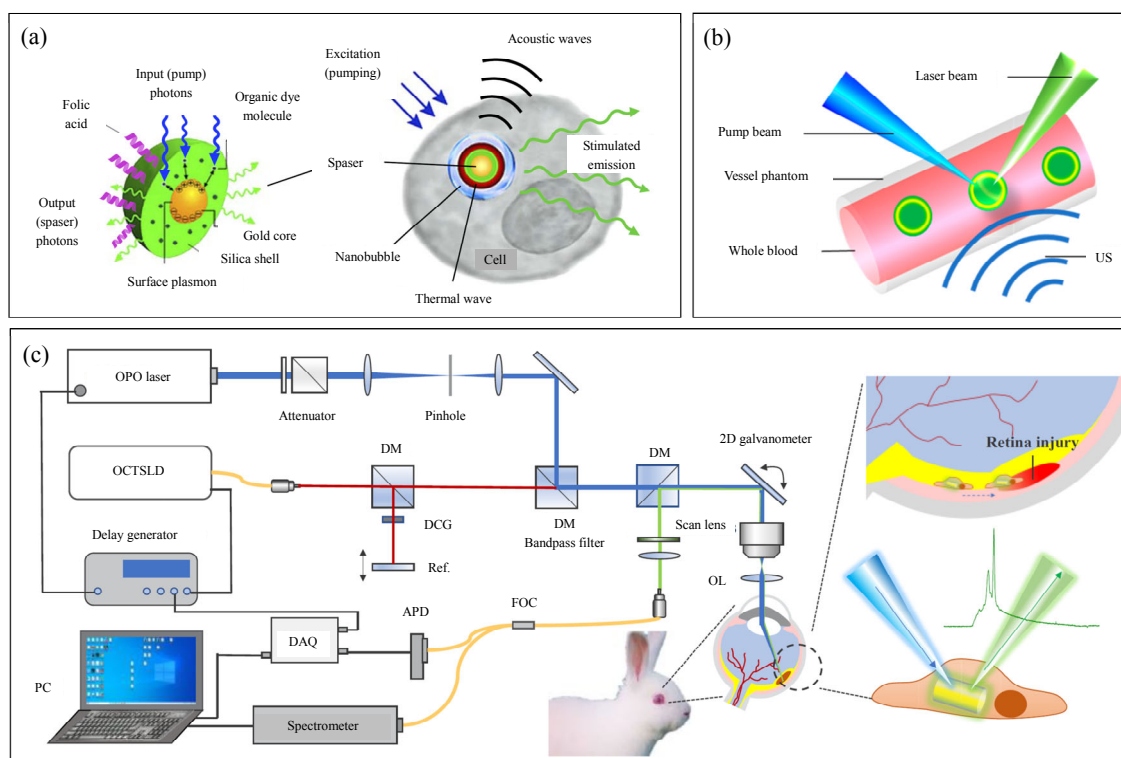


Fig. 12 Multimodal imaging and sensing with nanoparticles, droplets, and nanowire lasers: (a) schematic of spasers as multimodal cellular probes [213]; (b) schematic of ultrasound modulated droplet lasers in blood [218]; (c) multimodal imaging system combining OCT, FM, and laser labeling, with nanowire lasers serving as contrast agents and cell barcodes [220].

simultaneously [219]. Later in 2022, utilizing nanowire lasers as intracellular barcodes and contrast agents, a multimodal imaging system combining OCT, FM, and laser labeling was developed for 3D long-term tracking of individual cells in-vivo rabbit eyes [Fig. 12(c)] [220]. Besides, the multimodal detection concept can be extended from imaging to sensing. For example, optomechanical microcavities, which enable interactions between optical and mechanical resonance, provide an ideal platform for precision sensing of multiple physical quantities [221, 222]. And optomechanical lasers (e.g., phonon lasers that generate coherent sound oscillations [223]) are emerging as promising candidates for a variety of applications, such as simultaneously sensing light, sound, and microwave in a multi-physical environment [224, 225], offering unique opportunities for leveraging advantages of photon and phonon lasing to achieve the best of both worlds [226]. However, applications of these optomechanical cavities or lasers in biomolecular sensing and biomedical analysis are still in their early stages, calling for more research to realize their full potential.

## 6. Conclusion and outlooks

In summary, we review the basic building blocks for micro/nano lasers with their applications in biomolecular sensing and cellular analysis. As a new class of coherent light sources on the wavelength or sub-wavelength scale with good biocompatibility, micro/nano lasers offer unique ability to realize strong spatial and temporal confinement of light simultaneously, opening new opportunities for bio-applications at the molecular, cellular, and tissue level. At the molecular level, the biomolecular sensing with micro/nano lasers is highly desired for clinical diagnostics and life-science research. Its sensitivity can be greatly boosted due to the enhanced light-matter interaction that stems from the high  $Q$ -factor and small mode volume, and a high figure-of-merit and signal-to-noise ratio can be

achieved owing to the laser characteristics, including the narrow linewidth and high brightness, highlighting its potential for trace analysis, single-molecule detection, and biomolecular interaction studies. Besides the visible and near-infrared regime mainly focused in this review, the concept of micro/nano laser sensing may be extended to the mid-infrared range, a “fingerprint region” where various molecules undergo characteristic vibrational transitions, offering a possible avenue not only for identifications and quantifications of these molecules but also for getting deeper insights into their structures and activities. At the cellular and tissue levels, micro/nano lasers, which are capable of generating stimulated emission inside living cells and tissues with an unambiguous spectral definition and excellent background suppression, enable spectral multiplexing and bioimaging with spatial resolution beyond the diffraction limit, providing a versatile and promising platform for single-cell analysis, cell/tissue differentiation, and cancer diagnosis.

These remarkable advantages aside, several aspects of micro/nano lasers still need to be considered for bio-applications. First, to eliminate the biological perturbations and enhance spatial resolution as biological probes, shrinking the size of micro/nano lasers is of great demands, while challenges emerge as spatial scales decrease. For dielectric cavities,  $Q$ -factors are usually compromised with their size well below the diffraction limit, except for a few structures such as PhCs, which include periodic patterns that often have a feature volume larger than  $\lambda^3$  and add the complexity in fabrications. A possible approach to alleviate this issue is to utilize plasmon nano lasers, in which a 22-nm spaser has been demonstrated for intracellular probing [111]. However, the applications of spasers in cellular analysis are still in the infancy with many aspects waiting to be explored.

Second, for applications such as cell labeling

and tracking, since the cell migration may lead to rotation of the laser particles, the omnidirectional LE is quite needed, while the far-field emission of the conventional microlasers is usually intrinsically of high-directionality. Implementing boundary defects or scattering on semiconductor microdisk lasers has been proven to be effective [67], while applications using other laser types has yet to be explored.

Third, for in-vivo sensing using micro/nano lasers, it is still challenging for achieving high sensitivity; state-of-the-art micro/nanolaser sensors demonstrated in living cells usually have the RI sensitivity below 100 nm/RIU (e.g., the RI sensitivity of 50 nm/RIU–80 nm/RIU for intracellular laser sensors using semiconductor micro/nano disks or NWs [16, 20, 47]), which is much lower than their in-vitro counterparts using PhC or surface plasmon sensing. Further improvement of the bulk and surface sensitivity of these tiny intracellular laser sensors is thus in great demand.

Fourth, for implementation of micro/nano lasers based sensors in clinical applications from the concept of proof, several other challenges, including the long-term photostability or/and chemical-stability of the gain medium and background interference in the complex aqueous environment, ask for continuous efforts in searching novel materials and developing more sensing mechanisms.

Finally, incorporating biomaterials into micro/nano lasers provides a unique and promising platform to precisely control and modulate laser properties by biological molecules and processes (e.g., DNA sequences) [32, 204, 205], paving a way to versatile bio-switchable and bio-programmable photonic devices at the micro/nano scale. Meanwhile, benefitting from high  $Q$ -factors and small mode volumes, as well as the ability to control the laser gain medium using biomolecules, it will be interesting to explore micro/nano lasers generated from only a few or even single gain molecules [43, 227], which may enable ultrasensitive

biomolecule detection down to the single-molecule level [228], and provide insight into single-molecule physics, chemistry, and biology.

## Appendix

Table 2 References for the tree plot in Fig. 1.

Tree root	Ref.	Branch 1: sensing strategies	Ref.
WGM lasers	[8–10]	Laser intensity/peaks/thresholds	[1, 3, 8, 10]
F-P lasers	[33, 70, 76, 77]	Laser onset time	[13, 46]
NW lasers	[2, 78, 80]	Chirality	[161]
Random lasers	[12, 175, 198]	Polarization	[75]
PhC lasers	[98, 100, 101]	Transverse modes	[119, 120, 160, 217]
Plasmonic lasers	[5, 107, 132]		
Branch 2: sensing mechanisms	Ref.	Branch 3: biological analytes	Ref.
RI-induced	[1, 3, 8, 10]	DNA	[23, 24, 204–206]
FRET	[23, 32, 41, 50, 157, 204]	Protein	[13, 41, 44, 46, 151, 152, 159]
ELISA	[13, 46]	Exosome	[153]
Enzyme inhibition	[45, 145]	Virus	[8, 207, 208]
TIIA	[146, 159]	Bacteria	[37, 209–211]
Branch 4: laser probes	Ref.	Branch 5: imaging/mapping	Ref.
Microspheres	[15, 21, 34, 214]	Single cells mapping	[26, 215–217, 219, 220]
Semiconductor or NWs	[20, 57–59]	Tissue imaging	[69, 158, 181, 183]
Semiconductor or disks	[16, 47, 67]	Cancer screening	[14, 27, 182, 184, 216]
Spasers	[213]		

## Acknowledgment

This work was supported by the National Natural Science Foundation of China (Nos. 62005031 and 62005032), National Foreign Experts Program (No. DL2023165003L), and Innovation Support Plan for Returned Overseas Scholars (No. cx2021058) to Xiaoqin WU and Yipei WANG, and the Richard A. Auhll Endowed Professorship to Xudong FAN.

## Declarations

**Conflict of Interest** Xudong FAN is a co-inventor of some of the biolaser devices described in this article. The related technologies are licensed to LEMX Health Technology Co., LTD. Xudong FAN has financial interest in LEMX Health Technology Co., LTD.



**Permissions** All the included figures, tables, or text passages that have already been published elsewhere have obtained the permission from the copyright owner(s) for both the print and online format.

**Open Access** This article is distributed under the terms of the Creative Commons Attribution 4.0 International License (<http://creativecommons.org/licenses/by/4.0/>), which permits unrestricted use, distribution, and reproduction in any medium, provided you give appropriate credit to the original author(s) and the source, provide a link to the Creative Commons license, and indicate if changes were made.

## References

- [1] X. Fan and S. H. Yun, “The potential of optofluidic biolasers,” *Nature Methods*, 2014, 11(2): 141–147.
- [2] S. W. Eaton, A. Fu, A. B. Wong, C. Z. Ning, and P. Yang, “Semiconductor nanowire lasers,” *Nature Reviews Materials*, 2016, 1(6): 1–11.
- [3] Y. C. Chen and X. Fan, “Biological lasers for biomedical applications,” *Advanced Optical Materials*, 2019, 7(17): 1900377.
- [4] S. J. J. Kwok, N. Martino, P. H. Dannenberg, and S. H. Yun, “Multiplexed laser particles for spatially resolved single-cell analysis,” *Light: Science & Applications*, 2019, 8(1): 74.
- [5] R. M. Ma and R. F. Oulton, “Applications of nanolasers,” *Nature Nanotechnology*, 2019, 14(1): 12–22.
- [6] V. D. Ta, Y. Wang, and H. Sun, “Microlasers enabled by soft-matter technology,” *Advanced Optical Materials*, 2019, 7(17): 1900057.
- [7] K. Y. Jeong, M. S. Hwang, J. Kim, J. S. Park, J. M. Lee, and H. G. Park, “Recent progress in nanolaser technology,” *Advanced Materials*, 2020, 32(51): 2001996.
- [8] N. Toropov, G. Cabello, M. P. Serrano, R. R. Gutha, M. Rafti, and F. Vollmer, “Review of biosensing with whispering-gallery mode lasers,” *Light: Science & Applications*, 2021, 10(1): 1–19.
- [9] N. Toropov and F. Vollmer, “Whispering-gallery microlasers for cell tagging and barcoding: the prospects for in vivo biosensing,” *Light: Science & Applications*, 2021, 10(1): 77.
- [10] X. Yang, C. Gong, C. Zhang, Y. Wang, G. Yan, L. Wei, *et al.*, “Fiber optofluidic microlasers: Structures, characteristics, and applications,” *Laser & Photonics Reviews*, 2022, 16(1): 2100171.
- [11] H. Deng, G. L. Lippi, J. Mørk, J. Wiersig, and S. Reitzenstein, “Physics and applications of high- $\beta$  micro- and nanolasers,” *Advanced Optical Materials*, 2021, 9(19): 2100415.
- [12] D. Ni, M. Späth, F. Klämpfl, and M. Hohmann, “Properties and applications of random lasers as emerging light sources and optical sensors: a review,” *Sensors*, 2023, 23(1): 247.
- [13] X. Wu, M. K. K. Oo, K. Reddy, Q. Chen, Y. Sun, and X. Fan, “Optofluidic laser for dual-mode sensitive biomolecular detection with a large dynamic range,” *Nature Communications*, 2014, 5: 3779.
- [14] Y. C. Chen, X. Tan, Q. Sun, Q. Chen, W. Wang, and X. Fan, “Laser-emission imaging of nuclear biomarkers for high-contrast cancer screening and immunodiagnosis,” *Nature Biomedical Engineering*, 2017, 1(9): 724–735.
- [15] M. Schubert, L. Woolfson, I. R. M. Barnard, A. M. Dorward, B. Casement, A. Morton, *et al.*, “Monitoring contractility in cardiac tissue with cellular resolution using biointegrated microlasers,” *Nature Photonics*, 2020, 14(7): 452–458.
- [16] N. Martino, S. J. J. Kwok, A. C. Liapis, S. Forward, H. Jang, H. M. Kim, *et al.*, “Wavelength-encoded laser particles for massively multiplexed cell tagging,” *Nature Photonics*, 2019, 13(10): 720–727.
- [17] E. Heydari, J. Buller, E. Wischerhoff, A. Laschewsky, S. Döring, and J. Stumpe, “Label-free biosensor based on an all-polymer DFB laser,” *Advanced Optical Materials*, 2014, 2(2): 137–141.
- [18] M. Karl, J. M. E. Glackin, M. Schubert, N. M. Kronenberg, G. A. Turnbull, I. D. W. Samuel, *et al.*, “Flexible and ultra-lightweight polymer membrane lasers,” *Nature Communications*, 2018, 9(1): 1525.
- [19] X. Wu, Q. Chen, P. Xu, L. Tong, and X. Fan, “Refractive index sensing based on semiconductor nanowire lasers,” *Applied Physics Letters*, 2017, 111(3): 031112.
- [20] X. Wu, Q. Chen, P. Xu, Y. C. Chen, B. Wu, R. M. Coleman, *et al.*, “Nanowire lasers as intracellular probes,” *Nanoscale*, 2018, 10(20): 9729–9735.
- [21] M. Schubert, A. Steude, P. Liehm, N. M. Kronenberg, M. Karl, E. C. Campbell, *et al.*, “Lasing within live cells containing intracellular optical microresonators for barcode-type cell tagging and tracking,” *Nano Letters*, 2015, 15(8): 5647–5652.
- [22] W. Lee and X. Fan, “Intracavity DNA melting analysis with optofluidic lasers,” *Analytical Chemistry*, 2012, 84(21): 9558–9563.
- [23] Y. Sun and X. Fan, “Distinguishing DNA by analog-to-digital-like conversion by using optofluidic lasers,” *Angewandte Chemie – International Edition*, 2012, 51(5): 1236–1239.
- [24] W. Lee, Q. Chen, X. Fan, and D. K. Yoon, “Digital DNA detection based on a compact optofluidic laser with ultra-low sample consumption,” *Lab on a Chip*, 2016, 16(24): 4770–4776.
- [25] M. Hou, X. Liang, T. Zhang, C. Qiu, J. Chen, S. Liu, *et al.*, “DNA melting analysis with optofluidic lasers based on Fabry-Perot microcavity,” *ACS Sensors*, 2018, 3(9): 1750–1755.

- [26] Q. Chen, Y. C. Chen, Z. Zhang, B. Wu, R. Coleman, and X. Fan, "An integrated microwell array platform for cell lasing analysis," *Lab on a Chip*, 2017, 17(16): 2814–2820.
- [27] Y. C. Chen, Q. Chen, X. Tan, G. Chen, I. Bergin, M. N. Aslam, *et al.*, "Chromatin laser imaging reveals abnormal nuclear changes for early cancer detection," *Biomedical Optics Express*, 2019, 10(2): 838–854.
- [28] P. L. Gourley, "Semiconductor microlasers: a new approach to cell-structure analysis," *Nature Medicine*, 1996, 2(8): 942–944.
- [29] P. L. Gourley, A. E. McDonald, J. K. Hendricks, G. C. Copeland, J. Hunter, O. Akhil, *et al.*, "Nanolaser/microfluidic bioChip for realtime tumor pathology," *Biomedical Microdevices*, 1999, 2(2): 111–122.
- [30] P. L. Gourley, "Biocavity laser for high-speed cell and tumour biology," *Journal of Physics D: Applied Physics*, 2003, 36(14): R228.
- [31] P. L. Gourley, J. K. Hendricks, A. E. McDonald, R. G. Copeland, K. E. Barrett, C. R. Gourley, *et al.*, "Ultrafast nanolaser flow device for detecting cancer in single cells," *Biomedical Microdevices*, 2005, 7(4): 331–339.
- [32] Y. Sun, S. I. Shopova, C. S. Wu, S. Arnold, and X. Fan, "Bioinspired optofluidic FRET lasers via DNA scaffolds," *Proceedings of the National Academy of Sciences of the United States of America*, 2010, 107(37): 16039–16042.
- [33] M. C. Gather and S. H. Yun, "Single-cell biological lasers," *Nature Photonics*, 2011, 5(7): 406–410.
- [34] M. Humar and S. H. Yun, "Intracellular microlasers," *Nature Photonics*, 2015, 9(9): 572–576.
- [35] M. C. Gather and S. H. Yun, "Bio-optimized energy transfer in densely packed fluorescent protein enables near-maximal luminescence and solid-state lasers," *Nature Communications*, 2014, 5(1): 5722.
- [36] W. Zhang, J. Yao, and Y. S. Zhao, "Organic micro/nanoscale lasers," *Accounts of Chemical Research*, 2016, 49(9): 1691–1700.
- [37] T. Pan, D. Lu, H. Xin, and B. Li, "Biophotonic probes for bio-detection and imaging," *Light: Science & Applications*, 2021, 10(1): 124.
- [38] E. A. Prasetyanto, H. S. Wasisto, and D. Septiadi, "Cellular lasers for cell imaging and biosensing," *Acta Biomaterialia*, 2022, 143: 39–51.
- [39] P. Sarbadhikary, B. P. George, and H. Abrahamse, "Paradigm shift in future biophotonics for imaging and therapy: miniature living lasers to cellular scale optoelectronics," *Theranostics*, 2022, 12(17): 7335–7350.
- [40] H. Shan, H. Dai, and X. Chen, "Monitoring various bioactivities at the molecular, cellular, tissue, and organism levels via biological lasers," *Sensors*, 2022, 22(9): 3149.
- [41] Q. Chen, X. Zhang, Y. Sun, M. Ritt, S. Sivaramakrishnan, and X. Fan, "Highly sensitive fluorescent protein FRET detection using optofluidic lasers," *Lab on a Chip*, 2013, 13(14): 2679–2681.
- [42] X. Wu, Q. Chen, Y. Sun, and X. Fan, "Bio-inspired optofluidic lasers with luciferin," *Applied Physics Letters*, 2013, 102(20): 203706.
- [43] Q. Chen, M. Ritt, S. Sivaramakrishnan, Y. Sun, and X. Fan, "Optofluidic lasers with a single molecular layer of gain," *Lab on a Chip*, 2014, 14(24): 4590–4595.
- [44] Y. C. Chen, Q. Chen, and X. Fan, "Lasing in blood," *Optica*, 2016, 3(8): 809.
- [45] C. Gong, Y. Gong, M. K. K. Oo, Y. Wu, Y. Rao, X. Tan, *et al.*, "Sensitive sulfide ion detection by optofluidic catalytic laser using horseradish peroxidase (HRP) enzyme," *Biosensors & Bioelectronics*, 2017, 96: 351–357.
- [46] X. Tan, Q. Chen, H. Zhu, S. Zhu, Y. Gong, X. Wu, *et al.*, "Fast and reproducible ELISA laser platform for ultrasensitive protein quantification," *ACS Sensors*, 2020, 5(1): 110–117.
- [47] A. H. Fikouras, M. Schubert, M. Karl, J. D. Kumar, S. J. Powis, A. Di Falco, *et al.*, "Non-obstructive intracellular nanolasers," *Nature Communications*, 2018, 9(1): 4817.
- [48] C. Foucher, B. Guilhabert, J. Herrnsdorf, N. Laurand, and M. D. Dawson, "Diode-pumped, mechanically-flexible polymer DFB laser encapsulated by glass membranes," *Optics Express*, 2014, 22(20): 24160–24168.
- [49] C. S. Wu, M. K. K. Oo, and X. Fan, "Highly sensitive multiplexed heavy metal detection using quantum-dot-labeled DNazymes," *ACS Nano*, 2010, 4(10): 5897–5904.
- [50] Q. Chen, A. Kiraz, and X. Fan, "Optofluidic FRET lasers using aqueous quantum dots as donors," *Lab on a Chip*, 2016, 16(2): 353–359.
- [51] L. Yang, T. Carmon, B. Min, S. M. Spillane, and K. J. Vahala, "Erbium-doped and Raman microlasers on a silicon chip fabricated by the sol-gel process," *Applied Physics Letters*, 2005, 86(9): 091114.
- [52] B. Zhou, B. Shi, D. Jin, and X. Liu, "Controlling upconversion nanocrystals for emerging applications," *Nature Nanotechnology*, 2015, 10(11): 924–936.
- [53] M. J. Schnermann, "Organic dyes for deep bioimaging," *Nature*, 2017, 551(7679): 176–177.
- [54] S. Nizamoglu, M. C. Gather, and S. H. Yun, "All-biomaterial laser using vitamin and biopolymers," *Advanced Materials*, 2013, 25(41): 5943–5947.
- [55] H. J. Oh, M. C. Gather, J. J. Song, and S. H. Yun, "Lasing from fluorescent protein crystals," *Optics Express*, 2014, 22(25): 31411–31416.
- [56] E. A. Anashkina, "Laser sources based on rare-earth ion doped tellurite glass fibers and microspheres,"

- Fibers*, 2020, 8(5): 30.
- [57] R. Yan, J. H. Park, Y. Choi, C. J. Heo, S. M. Yang, L. P. Lee, *et al.*, “Nanowire-based single-cell endoscopy,” *Nature Nanotechnology*, 2012, 7(3): 191–196.
- [58] G. Shambat, S. R. Kothapalli, J. Provine, T. Sarmiento, J. Harris, S. S. Gambhir, *et al.*, “Single-cell photonic nanocavity probes,” *Nano Letters*, 2013, 13(11): 4999–5005.
- [59] S. Cho, M. Humar, N. Martino, and S. H. Yun, “Laser particle stimulated emission microscopy,” *Physical Review Letters*, 2016, 117(19): 193902.
- [60] M. Saldutti, M. Xiong, E. Dimopoulos, Y. Yu, M. Gioannini, and J. Mørk, “Modal properties of photonic crystal cavities and applications to lasers,” *Nanomaterials*, 2021, 11(11): 3030.
- [61] D. Conteduca, C. Reardon, M. G. Scullion, F. Dell’Olio, M. N. Armenise, T. F. Krauss, *et al.*, “Ultra-high  $Q/V$  hybrid cavity for strong light-matter interaction,” *APL Photonics*, 2017, 2(8): 086101.
- [62] Z. Yuan, X. Cheng, T. Li, Y. Zhou, Y. Zhang, X. Gong, *et al.*, “Light-harvesting in biophotonic optofluidic microcavities via whispering-gallery modes,” *ACS Applied Materials & Interfaces*, 2021, 13(31): 36909–36918.
- [63] S. Zhao, G. Li, X. Peng, J. Ma, Z. Yin, and Q. Zhao, “Ultralow-threshold green fluorescent protein laser based on high  $Q$  microbubble resonators,” *Optics Express*, 2022, 30(13): 23439–23447.
- [64] J. Ma, S. Zhao, X. Peng, G. Li, Y. Wang, B. Zhang, *et al.*, “An mCherry biolaser based on microbubble cavity with ultra-low threshold,” *Applied Physics Letters*, 2023, 123(5): 054103.
- [65] P. Wang, Y. Wang, Z. Yang, X. Guo, X. Lin, X. C. Yu, *et al.*, “Single-band 2-nm-line-width plasmon resonance in a strongly coupled Au nanorod,” *Nano Letters*, 2015, 15(11): 7581–7586.
- [66] C. Z. Ning, “Semiconductor nanolasers and the size-energy-efficiency challenge: a review,” *Advanced Photonics*, 2019, 1(01): 1.
- [67] S. J. Tang, P. H. Dannenberg, A. C. Liapis, N. Martino, Y. Zhuo, Y. F. Xiao, *et al.*, “Laser particles with omnidirectional emission for cell tracking,” *Light: Science & Applications*, 2021, 10(1): 23.
- [68] Y. Zhang, C. Hamsen, J. T. Choy, Y. Huang, J. H. Ryou, R. D. Dupuis, *et al.*, “Photonic crystal disk lasers,” *Optics Letters*, 2011, 36(14): 2704.
- [69] Y. C. Chen, Q. Chen, T. Zhang, W. Wang, and X. Fan, “Versatile tissue lasers based on high- $Q$  Fabry-Perot microcavities,” *Lab on a Chip*, 2017, 17(3): 538–548.
- [70] W. Wang, C. Zhou, T. Zhang, J. Chen, S. Liu, and X. Fan, “Optofluidic laser array based on stable high- $Q$  Fabry-Pérot microcavities,” *Lab on a Chip*, 2015, 15(19): 3862–3869.
- [71] P. R. Dolan, G. M. Hughes, F. Grazioso, B. R. Patton, and J. M. Smith, “Femtoliter tunable optical cavity arrays,” *Optics Letters*, 2010, 35(21): 3556–3558.
- [72] D. Hunger, T. Steinmetz, Y. Colombe, C. Deutsch, T. W. Hänsch, and J. Reichel, “A fiber Fabry-Perot cavity with high finesse,” *New Journal of Physics*, 2010, 12(6): 065038.
- [73] A. Muller, E. B. Flagg, J. R. Lawall, and G. S. Solomon, “Ultrahigh-finesse, low-mode-volume Fabry-Perot microcavity,” *Optics Letters*, 2010, 35(13): 2293–2295.
- [74] A. A. P. Trichet, P. R. Dolan, D. James, G. M. Hughes, C. Vallance, and J. M. Smith, “Nanoparticle trapping and characterization using open microcavities,” *Nano Letters*, 2016, 16(10): 6172–6177.
- [75] Z. Yuan, X. Cheng, Y. Zhou, X. Tan, X. Gong, H. Rivy, *et al.*, “Distinguishing small molecules in microcavity with molecular laser polarization,” *ACS Photonics*, 2020, 7(8): 1908–1914.
- [76] X. Wu, Q. Chen, Y. Wang, X. Tan, and X. Fan, “Stable high- $Q$  bouncing ball modes inside a Fabry-Pérot cavity,” *ACS Photonics*, 2019, 6(10): 2470–2478.
- [77] X. Wu, Y. Wang, Q. Chen, Y. C. Chen, X. Li, L. Tong, *et al.*, “High- $Q$ , low-mode-volume microsphere-integrated Fabry-Perot cavity for optofluidic lasing applications,” *Photonics Research*, 2019, 7(1): 50.
- [78] Y. Ma, X. Guo, X. Wu, L. Dai, and L. Tong, “Semiconductor nanowire lasers,” *Advances in Optics and Photonics*, 2013, 5(3): 216.
- [79] X. Guo, Y. Ma, Y. Wang, and L. Tong, “Nanowire plasmonic waveguides, circuits and devices,” *Laser & Photonics Reviews*, 2013, 7(6): 855–881.
- [80] M. H. Zhuge, C. Pan, Y. Zheng, J. Tang, S. Ullah, Y. Ma, *et al.*, “Wavelength-tunable micro/nanolasers,” *Advanced Optical Materials*, 2019, 7(17): 1900275.
- [81] S. Wang, Z. Hu, H. Yu, W. Fang, M. Qiu, and L. Tong, “Endface reflectivities of optical nanowires,” *Optics Express*, 2009, 17(13): 10881–10886.
- [82] X. Wu and Y. Wang, “A physics-based machine learning approach for modeling the complex reflection coefficients of metal nanowires,” *Nanotechnology*, 2022, 33(20): 205701.
- [83] X. Guo, Y. Ying, and L. Tong, “Photonic nanowires: From subwavelength waveguides to optical sensors,” *Accounts of Chemical Research*, 2014, 47(2): 656–666.
- [84] H. Wei, D. Pan, S. Zhang, Z. Li, Q. Li, N. Liu, *et al.*, “Plasmon waveguiding in nanowires,” *Chemical Reviews*, 2018, 118(6): 2882–2926.
- [85] Y. Wang, X. Wu, and P. Wang, “Asymmetric cavity mode engineering in a single plasmonic nanowire,” *Journal of Lightwave Technology*, 2021, 39(18): 5855–5863.
- [86] Y. Wang, Y. Ma, X. Guo, and L. Tong, “Single-mode plasmonic waveguiding properties of

- metal nanowires with dielectric substrates,” *Optics Express*, 2012, 20(17): 19006.
- [87] S. Zhang and H. Xu, “Optimizing substrate-mediated plasmon coupling toward high-performance plasmonic nanowire waveguides,” *ACS Nano*, 2012, 6(9): 8128–8135.
- [88] Y. Wang, Y. Feng, L. Zeng, and X. Wu, “Versatile and high-quality manipulation of asymmetric modes in bent metal nanowires,” *Optical Materials Express*, 2022, 12(7): 2782.
- [89] S. Nauert, A. Paul, Y. R. Zhen, D. Solis, L. Vigderman, W. S. Chang, *et al.*, “Influence of cross sectional geometry on surface plasmon polariton propagation in gold nanowires,” *ACS Nano*, 2014, 8(1): 572–580.
- [90] A. Luo, Y. Feng, C. Zhu, Y. Wang, and X. Wu, “Transfer learning for modeling plasmonic nanowire waveguides,” *Nanomaterials*, 2022, 12(20): 3624.
- [91] Y. Wang, A. Luo, C. Zhu, Z. Li, and X. Wu, “Ultra-confined propagating exciton–plasmon polaritons enabled by cavity-free strong coupling: Beating plasmonic trade-offs,” *Nanoscale Research Letters*, 2022, 17(1): 109.
- [92] H. Wu, L. Yang, P. Xu, J. Gong, X. Guo, P. Wang, *et al.*, “Photonic nanolaser with extreme optical field confinement,” *Physical Review Letters*, 2022, 129(1): 013902.
- [93] Y. Xiao, C. Meng, P. Wang, Y. Ye, H. Yu, S. Wang, *et al.*, “Single-nanowire single-mode laser,” *Nano Letters*, 2011, 11(3): 1122–1126.
- [94] Z. Hu, X. Guo, and L. Tong, “Freestanding nanowire ring laser,” *Applied Physics Letters*, 2013, 103(18): 183104.
- [95] X. Wu and L. Tong, “Optical microfibers and nanofibers,” *Nanophotonics*, 2013, 2(5–6): 407–428.
- [96] Y. Wang, X. Guo, L. Tong, and J. Lou, “Modeling of Au-nanowire waveguide for plasmonic sensing in liquids,” *Journal of Lightwave Technology*, 2014, 32(21): 4233–4238.
- [97] L. Tong, “Micro/nanofibre optical sensors: challenges and prospects,” *Sensors*, 2018, 18(3): 903.
- [98] S. Kita, K. Nozaki, S. Hachuda, H. Watanabe, Y. Saito, S. Otsuka, *et al.*, “Photonic crystal point-shift nanolasers with and without nanoslots – design, fabrication, lasing, and sensing characteristics,” *IEEE Journal of Selected Topics in Quantum Electronics*, 2011, 17(6): 1632–1647.
- [99] J. Xavier, S. Vincent, F. Meder, and F. Vollmer, “Advances in optoplasmonic sensors – combining optical nano/microcavities and photonic crystals with plasmonic nanostructures and nanoparticles,” *Nanophotonics*, 2018, 7(1): 1–38.
- [100] T. Baba, “Photonic and iontronic sensing in GaInAsP semiconductor photonic crystal nanolasers,” *Photonics*, 2019, 6(2): 65.
- [101] Q. Shi, J. Zhao, and L. Liang, “Two dimensional photonic crystal slab biosensors using label free refractometric sensing schemes: a review,” *Progress in Quantum Electronics*, 2021, 77: 100298.
- [102] M. Notomi, “Manipulating light with strongly modulated photonic crystals,” *Reports on Progress in Physics*, 2010, 73(9): 096501.
- [103] J. E. Baker, R. Sriram, and B. L. Miller, “Recognition-mediated particle detection under microfluidic flow with waveguide-coupled 2D photonic crystals: towards integrated photonic virus detectors,” *Lab on a Chip*, 2017, 17(9): 1570–1577.
- [104] K. Watanabe, M. Nomoto, F. Nakamura, S. Hachuda, A. Sakata, T. Watanabe, *et al.*, “Label-free and spectral-analysis-free detection of neuropsychiatric disease biomarkers using an ion-sensitive GaInAsP nanolaser biosensor,” *Biosensors and Bioelectronics*, 2018, 117: 161–167.
- [105] T. Asano, Y. Ochi, Y. Takahashi, K. Kishimoto, and S. Noda, “Photonic crystal nanocavity with a  $Q$  factor exceeding eleven million,” *Optics Express*, 2017, 25(3): 1769.
- [106] S. Hachuda, S. Otsuka, S. Kita, T. Isono, M. Narimatsu, K. Watanabe, *et al.*, “Selective detection of sub-atto-molar Streptavidin in  $10^{13}$ -fold impure sample using photonic crystal nanolaser sensors,” *Optics Express*, 2013, 21(10): 12815–12821.
- [107] R. M. Ma and S. Y. Wang, “Plasmonic nanolasers: fundamental properties and applications,” *Nanophotonics*, 2021, 10(14): 3623–3633.
- [108] H. Wu, Y. Gao, P. Xu, X. Guo, P. Wang, D. Dai, *et al.*, “Plasmonic nanolasers: pursuing extreme lasing conditions on nanoscale,” *Advanced Optical Materials*, 2019, 7(17): 1900334.
- [109] R. Chikkaraddy, B. de Nijs, F. Benz, S. J. Barrow, O. A. Scherman, E. Rosta, *et al.*, “Single-molecule strong coupling at room temperature in plasmonic nanocavities,” *Nature*, 2016, 535(7610): 127–130.
- [110] M. A. Noginov, G. Zhu, A. M. Belgrave, R. Bakker, V. M. Shalaev, E. E. Narimanov, *et al.*, “Demonstration of a spaser-based nanolaser,” *Nature*, 2009, 460(7259): 1110–1112.
- [111] E. I. Galanzha, R. Weingold, D. A. Nedosekin, M. Sarimollaoglu, J. Nolan, W. Harrington, *et al.*, “Spaser as a biological probe,” *Nature Communications*, 2017, 8(1): 15528.
- [112] M. P. Nezhad, A. Simic, O. Bondarenko, B. Slutsky, A. Mizrahi, L. Feng, *et al.*, “Room-temperature subwavelength metallo-dielectric lasers,” *Nature Photonics*, 2010, 4(6): 395–399.
- [113] S. H. Kwon, J. H. Kang, C. Seassal, S. K. Kim, P. Regreny, Y. H. Lee, *et al.*, “Subwavelength plasmonic lasing from a semiconductor nanodisk with silver nanopan cavity,” *Nano Letters*, 2010,

- 10(9): 3679–3683.
- [114] R. F. Oulton, V. J. Sorger, T. Zentgraf, R. M. Ma, C. Gladden, L. Dai, *et al.*, “Plasmon lasers at deep subwavelength scale,” *Nature*, 2009, 461(7264): 629–632.
- [115] R. M. Ma, R. F. Oulton, V. J. Sorger, G. Bartal, and X. Zhang, “Room-temperature sub-diffraction-limited plasmon laser by total internal reflection,” *Nature Materials*, 2011, 10(2): 110–113.
- [116] R. M. Ma, S. Ota, Y. Li, S. Yang, and X. Zhang, “Explosives detection in a lasing plasmon nanocavity,” *Nature Nanotechnology*, 2014, 9(8): 600–604.
- [117] X. Y. Wang, Y. L. Wang, S. Wang, B. Li, X. W. Zhang, L. Dai, *et al.*, “Lasing enhanced surface plasmon resonance sensing,” *Nanophotonics*, 2017, 6(2): 472–478.
- [118] X. Wu, Y. Xiao, C. Meng, X. Zhang, S. Yu, Y. Wang, *et al.*, “Hybrid photon-plasmon nanowire lasers,” *Nano Letters*, 2013, 13(11): 5654–5659.
- [119] C. Gong, Z. Qiao, Z. Yuan, S. H. Huang, W. Wang, P. C. Wu, *et al.*, “Topological encoded vector beams for monitoring amyloid-lipid interactions in microcavity,” *Advanced Science*, 2021, 8(12): 2100096.
- [120] C. Wang, C. Gong, Y. Zhang, Z. Qiao, Z. Yuan, Y. Gong, *et al.*, “Programmable rainbow-colored optofluidic fiber laser encoded with topologically structured chiral droplets,” *ACS Nano*, 2021, 15(7): 11126–11136.
- [121] M. Papič, U. Mur, K. P. Zuhail, M. Ravnik, I. Mušević, and M. Humar, “Topological liquid crystal superstructures as structured light lasers,” *Proceedings of the National Academy of Sciences of the United States of America*, 2021, 118(49): e2110839118.
- [122] M. Humar, M. Ravnik, S. Pajk, and I. Mušević, “Electrically tunable liquid crystal optical microresonators,” *Nature Photonics*, 2009, 3(10): 595–600.
- [123] M. Humar and I. Mušević, “Surfactant sensing based on whispering-gallery-mode lasing in liquid-crystal microdroplets,” *Optics Express*, 2011, 19(21): 19836.
- [124] H. Abbaszadeh, M. Fruchart, W. Van Saarloos, and V. Vitelli, “Liquid-crystal-based topological photonics,” *Proceedings of the National Academy of Sciences of the United States of America*, 2021, 118(4): e2020525118.
- [125] B. Zhen, C. W. Hsu, L. Lu, A. D. Stone, and M. Soljačić, “Topological nature of optical bound states in the continuum,” *Physical Review Letters*, 2014, 113(25): 257401.
- [126] S. I. Azzam and A. V. Kildishev, “Photonic bound states in the continuum: from basics to applications,” *Advanced Optical Materials*, 2021, 9(1): 2001469.
- [127] A. Kodigala, T. Lepetit, Q. Gu, B. Bahari, Y. Fainman, and B. Kanté, “Lasing action from photonic bound states in continuum,” *Nature*, 2017, 541(7636): 196–199.
- [128] C. Huang, C. Zhang, S. Xiao, Y. Wang, Y. Fan, Y. Liu, *et al.*, “Ultrafast control of vortex microlasers,” *Science*, 2020, 367(6481): 1018–1021.
- [129] Y. Ren, P. Li, Z. Liu, Z. Chen, Y. L. Chen, C. Peng, *et al.*, “Low-threshold nanolasers based on miniaturized bound states in the continuum,” *Science Advances*, 2022, 8(51): eade8817.
- [130] E. Kuramochi, M. Notomi, S. Mitsugi, A. Shinya, T. Tanabe, and T. Watanabe, “Ultrahigh- $Q$  photonic crystal nanocavities realized by the local width modulation of a line defect,” *Applied Physics Letters*, 2006, 88(4): 041112.
- [131] T. Watanabe, Y. Saijo, Y. Hasegawa, K. Watanabe, Y. Nishijima, and T. Baba, “Ion-sensitive photonic-crystal nanolaser sensors,” *Optics Express*, 2017, 25(20): 24469–24479.
- [132] S. I. Azzam, A. V. Kildishev, R. M. Ma, C. Z. Ning, R. Oulton, V. M. Shalae, *et al.*, “Ten years of spasers and plasmonic nanolasers,” *Light: Science & Applications*, 2020, 9(1): 90.
- [133] R. Matthes, C. P. Cain, and D. Courant, “Revision of guidelines on limits of exposure to laser radiation of wavelengths between 400 nm and 1.4  $\mu\text{m}$ ,” *Health Physics*, 2000, 79(4): 431–440.
- [134] H. Chandralalim and X. Fan, “Reconfigurable solid-state dye-doped polymer ring resonator lasers,” *Scientific Reports*, 2015, 5(1): 18310.
- [135] S. Lacey, I. M. White, Y. Sun, S. I. Shopova, J. M. Cupps, P. Zhang, *et al.*, “Versatile opto-fluidic ring resonator lasers with ultra-low threshold,” *Optics Express*, 2007, 15(23): 15523–15530.
- [136] H. Dai, B. Jiang, C. Yin, Z. Cao, and X. Chen, “Ultralow-threshold continuous-wave lasing assisted by a metallic optofluidic cavity exploiting continuous pump,” *Optics Letters*, 2018, 43(4): 847.
- [137] A. Fernandez-Bravo, K. Yao, E. S. Barnard, N. J. Borys, E. S. Levy, B. Tian, *et al.*, “Continuous-wave upconverting nanoparticle microlasers,” *Nature Nanotechnology*, 2018, 13(7): 572–577.
- [138] A. Fernandez-Bravo, D. Wang, E. S. Barnard, A. Teitelboim, C. Tajon, J. Guan, *et al.*, “Ultralow-threshold, continuous-wave upconverting lasing from subwavelength plasmons,” *Nature Materials*, 2019, 18(11): 1172–1176.
- [139] F. Xu, Y. C. Zhu, Z. Y. Ma, W. W. Zhao, J. J. Xu, and H. Y. Chen, “An ultrasensitive energy-transfer based photoelectrochemical protein biosensor,” *Chemical Communications*, 2016, 52(14): 3034–3037.

- [140] D. Etezadi, J. B. Warner IV, F. S. Ruggeri, G. Dietler, H. A. Lashuel, and H. Altug, "Nanoplasmonic mid-infrared biosensor for in vitro protein secondary structure detection," *Light: Science & Applications*, 2017, 6(8): e17029–e17029.
- [141] Z. Mazouz, M. Mokni, N. Fourati, C. Zerrouki, F. Barbault, M. Seydou, *et al.*, "Computational approach and electrochemical measurements for protein detection with MIP-based sensor," *Biosensors and Bioelectronics*, 2020, 151: 111978.
- [142] S. Aitekenov, A. Gaipov, and R. Bukasov, "Review: detection and quantification of proteins in human urine," *Talanta*, 2021, 223: 121718.
- [143] P. Niu, J. Jiang, K. Liu, S. Wang, T. Wang, Y. Liu, *et al.*, "High-sensitive and disposable myocardial infarction biomarker immunosensor with optofluidic microtubule lasing," *Nanophotonics*, 2022, 11(14): 3351–3364.
- [144] C. Gong, Y. Gong, Q. Chen, Y. J. Rao, G. D. Peng, and X. Fan, "Reproducible fiber optofluidic laser for disposable and array applications," *Lab on a Chip*, 2017, 17(20): 3431–3436.
- [145] C. Gong, Y. Gong, X. Zhao, Y. Luo, Q. Chen, X. Tan, *et al.*, "Distributed fibre optofluidic laser for chip-scale arrayed biochemical sensing," *Lab on a Chip*, 2018, 18(18): 2741–2748.
- [146] X. Yang, Y. Luo, Y. Liu, C. Gong, Y. Wang, Y. J. Rao, *et al.*, "Mass production of thin-walled hollow optical fibers enables disposable optofluidic laser immunosensors," *Lab on a Chip*, 2020, 20(5): 923–930.
- [147] X. Yang, C. Gong, Y. Wang, Y. Luo, Y. J. Rao, G. D. Peng, *et al.*, "A sequentially bioconjugated optofluidic laser for wash-out-free and rapid biomolecular detection," *Lab on a Chip*, 2021, 21(9): 1686–1693.
- [148] Z. Yuan, X. Tan, X. Gong, C. Gong, X. Cheng, S. Feng, *et al.*, "Bioresponsive microlasers with tunable lasing wavelength," *Nanoscale*, 2021, 13(3): 1608–1615.
- [149] X. Gong, Z. Qiao, P. Guan, S. Feng, Z. Yuan, C. Huang, *et al.*, "Hydrogel microlasers for versatile biomolecular analysis based on a lasing microarray," *Advanced Photonics Research*, 2020, 1(1): 2000041.
- [150] Z. Wang, Y. Zhang, X. Gong, Z. Yuan, S. Feng, T. Xu, *et al.*, "Bio-electrostatic sensitive droplet lasers for molecular detection," *Nanoscale Advances*, 2020, 2(7): 2713–2719.
- [151] K. K. Chan, L. W. Shang, Z. Qiao, Y. Liao, M. Kim, and Y. C. Chen, "Monitoring amyloidogenesis with a 3D deep-learning-guided biolaser imaging array," *Nano Letters*, 2022, 22(22): 8949–8956.
- [152] Z. Wang, Y. Liu, C. Gong, Z. Yuan, L. Shen, P. Chang, *et al.*, "Liquid crystal-amplified optofluidic biosensor for ultra-highly sensitive and stable protein assay," *Photonix*, 2021, 2(1): 18.
- [153] Z. Wang, G. Fang, Z. Gao, Y. Liao, C. Gong, M. Kim, *et al.*, "Autonomous microlasers for profiling extracellular vesicles from cancer spheroids," *Nano Letters*, 2023, 23(7): 2502–2510.
- [154] Y. Zhang, C. Zhang, Y. Fan, Z. Liu, F. Hu, and Y. S. Zhao, "Smart protein-based biolasers: an alternative way to protein conformation detection," *ACS Applied Materials & Interfaces*, 2021, 13(16): 19187–19192.
- [155] S. Caixeiro, C. Kunstmann-Olsen, M. Schubert, J. Hill, I. R. M. Barnard, M. D. Simmons, *et al.*, "Local sensing of absolute refractive index during protein-binding using microlasers with spectral encoding," *Advanced Optical Materials*, 2023, 11(13): 2300530.
- [156] A. Capocéfalo, S. Gentilini, L. Barolo, P. Baiocco, C. Conti, and N. Ghofraniha, "Biosensing with free space whispering gallery mode microlasers," *Photonics Research*, 2023, 11(5): 732.
- [157] M. Aas, Q. Chen, A. Jonas, A. Kiraz, and X. Fan, "Optofluidic FRET lasers and their applications in novel photonic devices and biochemical sensing," *IEEE Journal of Selected Topics in Quantum Electronics*, 2016, 22(4): 7000215.
- [158] Y. C. Chen, Q. Chen, X. Wu, X. Tan, J. Wang, and X. Fan, "A robust tissue laser platform for analysis of formalin-fixed paraffin-embedded biopsies," *Lab on a Chip*, 2018, 18(7): 1057–1065.
- [159] X. Yang, W. Shu, Y. Wang, Y. Gong, C. Gong, Q. Chen, *et al.*, "Turbidimetric inhibition immunoassay revisited to enhance its sensitivity via an optofluidic laser," *Biosensors & Bioelectronics*, 2019, 131: 60–66.
- [160] C. Gong, Z. Qiao, S. Zhu, W. Wang, and Y. C. Chen, "Self-assembled biophotonic lasing network driven by amyloid fibrils in microcavities," *ACS Nano*, 2021, 15(9): 15007–15016.
- [161] Z. Yuan, Y. Zhou, Z. Qiao, C. Eng Aik, W. C. Tu, X. Wu, *et al.*, "Stimulated chiral light-matter interactions in biological microlasers," *ACS Nano*, 2021, 15(5): 8965–8975.
- [162] R. Abe, T. Takeda, R. Shiratori, S. Shirakawa, S. Saito, and T. Baba, "Optimization of an H0 photonic crystal nanocavity using machine learning," *Optics Letters*, 2020, 45(2): 319–322.
- [163] Z. Li, Z. Zhang, A. Scherer, and D. Psaltis, "Mechanically tunable optofluidic distributed feedback dye laser," *Optics Express*, 2006, 14(22): 10494–10499.
- [164] Z. Li and D. Psaltis, "Optofluidic distributed feedback dye lasers," *IEEE Journal of Selected Topics in Quantum Electronics*, 2007, 13(2): 185–193.

- [165] M. Lu, S. S. Choi, U. Irfan, and B. T. Cunningham, "Plastic distributed feedback laser biosensor," *Applied Physics Letters*, 2008, 93(11): 111113.
- [166] M. Lu, S. S. Choi, C. J. Wagner, J. G. Eden, and B. T. Cunningham, "Label free biosensor incorporating a replica-molded, vertically emitting distributed feedback laser," *Applied Physics Letters*, 2008, 92(26): 261502.
- [167] C. Vannahme, M. C. Leung, F. Richter, C. L. C. Smith, P. G. Hermannsson, and A. Kristensen, "Nanoimprinted distributed feedback lasers comprising TiO<sub>2</sub> thin films: design guidelines for high performance sensing," *Laser & Photonics Reviews*, 2013, 7(6): 1036–1042.
- [168] A. Retolaza, J. Martinez-Perdiguero, S. Merino, M. Morales-Vidal, P. G. Boj, J. A. Quintana, *et al.*, "Organic distributed feedback laser for label-free biosensing of ErbB2 protein biomarker," *Sensors and Actuators B: Chemical*, 2016, 223: 261–265.
- [169] P. Zeng, Y. Zhou, B. Wang, X. Li, Q. Ou, X. Wu, *et al.*, "Nanoimprinted organic distributed feedback biosensors breaking the trade-off between sensitivity and threshold," *Organic Electronics*, 2020, 85: 105851.
- [170] Z. Li, Z. Zhang, T. Emery, A. Scherer, and D. Psaltis, "Single mode optofluidic distributed feedback dye laser," *Optics Express*, 2006, 14(2): 696–701.
- [171] A. M. Haughey, B. Guilhabert, A. L. Kanibolotsky, P. J. Skabara, G. A. Burley, M. D. Dawson, *et al.*, "An organic semiconductor laser based on star-shaped truxene-core oligomers for refractive index sensing," *Sensors and Actuators B: Chemical*, 2013, 185: 132–139.
- [172] M. Umar, K. Min, H. Jeon, and S. Kim, "Single-mode distributed feedback laser operation with no dependence on the morphology of the gain medium: single-mode distributed feedback laser operation," *Annalen der Physik*, 2017, 529(6): 1700034.
- [173] T. Sano, R. Losakul, and H. Schmidt, "Dual optofluidic distributed feedback dye lasers for multiplexed biosensing applications," *Scientific Reports*, 2023, 13(1): 16824.
- [174] T. Sano, H. Zhang, R. Losakul, and H. Schmidt, "All-in-one optofluidic chip for molecular biosensing assays," *Biosensors*, 2022, 12(7): 501.
- [175] S. Caixeiro, M. Gaio, B. Marelli, F. G. Omenetto, and R. Sapienza, "Silk-based biocompatible random lasing," *Advanced Optical Materials*, 2016, 4(7): 998–1003.
- [176] X. Liu, T. Li, T. Yi, C. Wang, J. Li, M. Xu, *et al.*, "Random laser action from a natural flexible biomembrane-based device," *Journal of Modern Optics*, 2016, 63(13): 1248–1253.
- [177] X. Li, F. Gong, D. Liu, S. He, H. Yuan, L. Dai, *et al.*, "A lotus leaf based random laser," *Organic Electronics*, 2019, 69: 216–219.
- [178] C. S. Wang, T. Y. Chang, T. Y. Lin, and Y. F. Chen, "Biologically inspired flexible quasi-single-mode random laser: an integration of *Pieris canidia* butterfly wing and semiconductors," *Scientific Reports*, 2014, 4: 6736.
- [179] S. W. Chen, J. Y. Lu, B. Y. Hung, M. Chiesa, P. H. Tung, J. H. Lin, *et al.*, "Random lasers from photonic crystal wings of butterfly and moth for speckle-free imaging," *Optics Express*, 2021, 29(2): 2065–2076.
- [180] F. Lahoz, A. Acebes, T. González-Hernández, S. de Armas-Rillo, K. Soler-Carracedo, G. Cuesto, *et al.*, "Random lasing in brain tissues," *Organic Electronics*, 2019, 75: 105389.
- [181] F. Lahoz, I. R. Martín, M. Urgellés, J. Marrero-Alonso, R. Marín, C. J. Saavedra, *et al.*, "Random laser in biological tissues impregnated with a fluorescent anticancer drug," *Laser Physics Letters*, 2015, 12(4): 045805.
- [182] Y. Wang, Z. Duan, Z. Qiu, P. Zhang, J. Wu, D. Zhang, *et al.*, "Random lasing in human tissues embedded with organic dyes for cancer diagnosis," *Scientific Reports*, 2017, 7(1): 8385.
- [183] M. Hohmann, D. Dörner, F. Mehari, C. Chen, M. Späth, S. Müller, *et al.*, "Investigation of random lasing as a feedback mechanism for tissue differentiation during laser surgery," *Biomedical Optics Express*, 2019, 10(2): 807–816.
- [184] D. Zhang, Y. Wang, J. Tang, and H. Mu, "Random laser marked PLCD1 gene therapy effect on human breast cancer," *Journal of Applied Physics*, 2019, 125(20): 203102.
- [185] M. Hohmann, M. Späth, D. Ni, D. Dörner, B. Lengenfelder, F. Klämpfl, *et al.*, "Random laser as a potential tool for the determination of the scattering coefficient," *Biomedical Optics Express*, 2021, 12(9): 5439–5451.
- [186] M. C. A. de Oliveira, F. W. S. de Sousa, F. A. Santos, L. M. G. Abegão, M. A. R. C. Alencar, J. J. Rodrigues, *et al.*, "Dye-doped electrospun fibers for use as random laser generator: The influence of spot size and scatter concentration," *Optical Materials*, 2020, 101: 109722.
- [187] F. Tommasi, E. Ignesti, L. Fini, F. Martelli, and S. Cavalieri, "Random laser based method for direct measurement of scattering properties," *Optics Express*, 2018, 26(21): 27615–27627.
- [188] T. Okamoto and S. Adachi, "Effect of particle size and shape on nonresonant random laser action of dye-doped polymer random media," *Optical Review*, 2010, 17(3): 300–304.
- [189] S. Ning, K. Dai, N. Zhang, Y. Zhang, Y. Wu, J. Huang, *et al.*, "Improving the random lasing performance using Au@SiO<sub>2</sub> nanocubes-silver film hybrid structure," *Journal of Luminescence*, 2021, 231: 117788.

- [190] J. Kitur, G. Zhu, M. Bahoura, and M. A. Noginov, "Dependence of the random laser behavior on the concentrations of dye and scatterers," *Journal of Optics*, 2010, 12(2): 024009.
- [191] Y. Li, K. Xie, X. Zhang, Z. Hu, J. Ma, X. Chen, *et al.*, "Coherent random lasing realized in polymer vesicles," *Photonic Sensors*, 2020, 10(3): 254–264.
- [192] J. Yi, G. Feng, L. Yang, K. Yao, C. Yang, Y. Song, *et al.*, "Behaviors of the Rh6G random laser comprising solvents and scatterers with different refractive indices," *Optics Communications*, 2012, 285(24): 5276–5282.
- [193] X. Meng, K. Fujita, S. Murai, J. Konishi, M. Mano, and K. Tanaka, "Random lasing in ballistic and diffusive regimes for macroporous silica-based systems with tunable scattering strength," *Optics Express*, 2010, 18(12): 12153–12160.
- [194] M. Gaio, S. Caixeiro, B. Marelli, F. G. Omenetto, and R. Sapienza, "Gain-based mechanism for pH sensing based on random lasing," *Physical Review Applied*, 2017, 7(3): 034005.
- [195] W. Z. W. Ismail, G. Liu, K. Zhang, E. M. Goldys, and J. M. Dawes, "Dopamine sensing and measurement using threshold and spectral measurements in random lasers," *Optics Express*, 2016, 24(2): A85–A91.
- [196] X. Shi, K. Ge, J. H. Tong, and T. Zhai, "Low-cost biosensors based on a plasmonic random laser on fiber facet," *Optics Express*, 2020, 28(8): 12233–12242.
- [197] Z. Xu, Q. Hong, K. Ge, X. Shi, X. Wang, J. Deng, *et al.*, "Random lasing from label-free living cells for rapid cytometry of apoptosis," *Nano Letters*, 2022, 22(1): 172–178.
- [198] J. He, S. Hu, J. Ren, X. Cheng, Z. Hu, N. Wang, *et al.*, "Biofluidic random laser cytometer for biophysical phenotyping of cell suspensions," *ACS Sensors*, 2019, 4(4): 832–840.
- [199] N. Mogharari and B. Sajad, "Random laser emission spectra of the normal and cancerous thyroid tissues," *Iranian Journal of Science and Technology, Transaction A: Science*, 2019, 43(4): 2055–2060.
- [200] A. N. Azmi, W. Z. Wan Ismail, H. Abu Hassan, M. M. Halim, N. Zainal, O. L. Muskens, *et al.*, "Review of open cavity random lasers as laser-based sensors," *ACS Sensors*, 2022, 7(4): 914–928.
- [201] A. T. H. Hsieh, P. J. H. Pan, and A. P. Lee, "Rapid label-free DNA analysis in picoliter microfluidic droplets using FRET probes," *Microfluidics and Nanofluidics*, 2009, 6(3): 391–401.
- [202] S. Song, Z. Liang, J. Zhang, L. Wang, G. Li, and C. Fan, "Gold-nanoparticle-based multicolor nanobeacons for sequence-specific DNA analysis," *Angewandte Chemie International Edition*, 2009, 48(46): 8670–8674.
- [203] C. M. Rodríguez López, B. Guzmán Asenjo, A. J. Lloyd, and M. J. Wilkinson, "Direct detection and quantification of methylation in nucleic acid sequences using high-resolution melting analysis," *Analytical Chemistry*, 2010, 82(21): 9100–9108.
- [204] X. Zhang, W. Lee, and X. Fan, "Bio-switchable optofluidic lasers based on DNA Holliday junctions," *Lab on a Chip*, 2012, 12(19): 3673–3675.
- [205] Q. Chen, H. Liu, W. Lee, Y. Sun, D. Zhu, H. Pei, *et al.*, "Self-assembled DNA tetrahedral optofluidic lasers with precise and tunable gain control," *Lab on a Chip*, 2013, 13(17): 3351–3354.
- [206] Y. Zhang, X. Gong, Z. Yuan, W. Wang, and Y. C. Chen, "DNA self-switchable microlaser," *ACS Nano*, 2020, 14(11): 16122–16130.
- [207] L. He, Ş. K. Özdemir, J. Zhu, W. Kim, and L. Yang, "Detecting single viruses and nanoparticles using whispering gallery microlasers," *Nature Nanotechnology*, 2011, 6(7): 428–432.
- [208] J. E. Hales, G. Matmon, P. A. Dalby, J. M. Ward, and G. Aeppli, "Virus lasers for biological detection," *Nature Communications*, 2019, 10(1): 3594.
- [209] M. C. Gather and S. H. Yun, "Lasing from Escherichia coli bacteria genetically programmed to express green fluorescent protein," *Optics Letters*, 2011, 36(16): 3299–3301.
- [210] A. Jonáš, M. Aas, Y. Karadag, S. Manioğlu, S. Anand, D. McGloin, *et al.*, "In vitro and in vivo biolasing of fluorescent proteins suspended in liquid microdroplet cavities," *Lab on a Chip*, 2014, 14(16): 3093–3100.
- [211] H. Altug, S. H. Oh, S. A. Maier, and J. Homola, "Advances and applications of nanophotonic biosensors," *Nature Nanotechnology*, 2022, 17(1): 5–16.
- [212] C. Feng, Z. Xu, X. Wang, H. Yang, L. Zheng, and H. Fu, "Organic-nanowire-SiO<sub>2</sub> core-shell microlasers with highly polarized and narrow emissions for biological imaging," *ACS Applied Materials & Interfaces*, 2017, 9(8): 7385–7391.
- [213] E. I. Galanzha, R. Weingold, D. A. Nedosekin, M. Sarimollaoglu, J. Nolan, W. Harrington, *et al.*, "Spaser as a biological probe," *Nature Communications*, 2017, 8(1): 15528.
- [214] M. Humar, A. Dobravec, X. Zhao, and S. H. Yun, "Biomaterial microlasers implantable in the cornea, skin, and blood," *Optica*, 2017, 4(9): 1080–1085.
- [215] Y. C. Chen, X. Li, H. Zhu, W. H. Weng, X. Tan, Q. Chen, *et al.*, "Monitoring neuron activities and interactions with laser emissions," *ACS Photonics*, 2020, 7(8): 2182–2189.
- [216] C. Gong, F. Sun, G. Yang, C. Wang, C. Huang, and Y. C. Chen, "Multifunctional laser imaging of cancer cell secretion with hybrid liquid crystal



- resonators,” *Laser & Photonics Reviews*, 2022, 16(8): 2100734.
- [217] Z. Qiao, H. Xu, N. Zhang, X. Gong, C. Gong, G. Yang, *et al.*, “Cellular features revealed by transverse laser modes in frequency domain,” *Advanced Science*, 2022, 9(1): 2270014.
- [218] X. Li, Y. Qin, X. Tan, Y. C. Chen, Q. Chen, W. H. Weng, *et al.*, “Ultrasound modulated droplet lasers,” *ACS Photonics*, 2019, 6(2): 531–537.
- [219] X. Li, W. Zhang, W. Y. Wang, X. Wu, Y. Li, X. Tan, *et al.*, “Optical coherence tomography and fluorescence microscopy dual-modality imaging for in vivo single-cell tracking with nanowire lasers,” *Biomedical Optics Express*, 2020, 11(7): 3659–3672.
- [220] X. Li, W. Zhang, Y. Li, X. Wu, M. Wang, X. Tan, *et al.*, “In vivo tracking of individual stem cells labeled with nanowire lasers using multimodality imaging,” *Biomedical Optics Express*, 2022, 13(9): 4706.
- [221] G. Bahl, K. H. Kim, W. Lee, J. Liu, X. Fan, and T. Carmon, “Brillouin cavity optomechanics with microfluidic devices,” *Nature Communications*, 2013, 4: 1994.
- [222] B. B. Li, L. Ou, Y. Lei, and Y. C. Liu, “Cavity optomechanical sensing,” *Nanophotonics*, 2021, 10(11): 2799–2832.
- [223] J. Zhang, B. Peng, Ş. K. Özdemir, K. Pichler, D. O. Krimer, G. Zhao, *et al.*, “A phonon laser operating at an exceptional point,” *Nature Photonics*, 2018, 12(8): 479–484.
- [224] J. Yang, T. Qin, F. Zhang, X. Chen, X. Jiang, and W. Wan, “Multiphysical sensing of light, sound and microwave in a microcavity Brillouin laser,” *Nanophotonics*, 2020, 9(9): 2915–2925.
- [225] H. Wisniewski, L. Richardson, A. Hines, A. Laurain, and F. Guzmán, “Optomechanical lasers for inertial sensing,” *Journal of the Optical Society of America A*, 2020, 37(9): B87–B92.
- [226] N. Wang, H. Wen, J. C. A. Zacarias, J. E. Antonio-Lopez, Y. Zhang, D. C. Delgado, *et al.*, “Laser<sup>2</sup>: a two-domain photon-phonon laser,” *Science Advances*, 2023, 9(26): eadg7841.
- [227] Z. S. Wang, H. A. Rabitz, and M. O. Scully, “The single-molecule dye laser,” *Laser Physics*, 2005, 15(1): 118–123.
- [228] C. Gong, X. Yang, S. J. Tang, Q. Q. Zhang, Y. Wang, Y. L. Liu, *et al.*, “Submonolayer biolasers for ultrasensitive biomarker detection,” *Light: Science & Applications*, 2023, 12: 292.